Doctor of Philosophy

Design and Performance Enhancement of a Gasoline Engine Turbocharger Compressor by Adopting RCT and Hybrid RCT

The Graduate School

of the University of Ulsan

School of Mechanical Engineering

Zhou Tianjun

Design and Performance Enhancement of a Gasoline Engine Turbocharger Compressor by Adopting RCT and Hybrid RCT

Supervisor: Pro. Geun Sik Lee

A Dissertation

Submitted to
The Graduate School of the University of Ulsan
In Partial Fulfillment of the Requirements
For the Degree of

Doctor of Philosophy

by

Zhou Tianjun

School of Mechanical Engineering
University of Ulsan
Ulsan, Korea
February 2019

Zhou Tianjun 의 공학박사 학위 논문을 인준함

심 사 위원장	이상욱	인
심 사 위 원	이근식	인
심 사 위 원	장경식	인
심 사 위 원	이목인	인
심 사 위 원	김찬중	인

울산대학교 대학원

기계공학부

2019 년 **02** 월

Design and Performance Enhancement of a Gasoline Engine Turbocharger Compressor by Adopting RCT and Hybrid RCT

This certifies that the dissertation

of Zhou Tianjun is approved.

Committee Chairman Prof. SANG WOOK LEE

Committee Member Prof. GEUN SIK LEE

Committee Member Prof. KYOUNG SIK CHANG

Committee Member Prof. MOKIN LEE

Committee Member Prof. CHARN JUNG KIM

School of Mechanical Engineering

University of Ulsan, Republic of Korea

February 2019

ACKNOWLEDGMENTS

First and foremost, I would like to show my deepest gratitude to my supervisor, Professor Dr. Geun Sik Lee, a respectable, responsible and resourceful scholar, who has provided me with valuable guidance in every stage of my Doctor course and this thesis. Without his enlightening instruction, impressive kindness and patience, I could not have completed my thesis. His keen and vigorous academic observation enlightens me not only in this thesis but also in my future study.

Sincerely thanks to the University of Ulsan that granted me the scholarship and opportunity for studying in Korea. I also express my gratitude to the professors and staff members of the School of Mechanical Engineering for their kindly helps.

Special thanks to all members of my laboratory who supported me a lot in my research work.

Finally, I would like to thank my parents, girlfriend, and friends, who have been there all the time, giving me support, encouragement and lighting up the time.

Ulsan 12/2018

Zhou Tianjun

Design and Performance Enhancement of a Gasoline Engine Turbocharger Compressor by Adopting RCT and Hybrid RCT

By

Zhou Tianjun

School of Mechanical Engineering

University of Ulsan

ABSTRACT

The diesel engine used the turbocharger technology for a long period. To solve the compressor associated with surge unstable phenomena, the medium and large size turbocharger compressor used the RCT(recirculation casing treatment) also called ported shroud technology in a diesel engine. The RCT can decrease the vortex at the impeller part when the compressor is operated in the low mass flow rate working fluid. Due to the casting limitation, the small size compressor which the pressure ratio range from 1.2 to 2.5 is not easy to adopt the RCT technology. The 3D printer technology has been developing very quickly nowadays. It can also be used for the future compressor production. Recently, the turbocharger has been installed to the gasoline engine to increase the engine power and

decrease the emission pollution. Most gasoline engine displacement is from 1.3L to 2.0L. Hence, it is essential to investigate the flow and performance of the small-sized gasoline engine turbocharger RCT compressor by using the CFD technology. Comparing the CFD results between the Non-RCT and RCT compressor model, the RCT compressor can increase the efficiency at the low mass flow rate, which improves the unstable flow performance. However, at the medium mass flow rate range, especially the mass flow rate of the gasoline engine at the highest power output point, the RCT compressor has the lower efficiency than the non-RCT compressor. A new Hybrid RCT has been designing by the author which has a small channel connecting the compressor volute downstream part and RCT inlet duct to improve the flow movement by overcoming the adverse pressure gradient. The CFD results showed that the Hybrid RCT compressor had a similar performance with the RCT compressor, but it could increase the efficiency than the RCT compressor at the medium mass flow range and showed higher efficiency in a certain region of compressor than the non-RCT compressor.

Keywords: Turbocharger, Compressor, Recirculating Casing Treatment, Pressure Ratio, Efficiency, Surge

CONTENTS

LIST OF FIGURES

LIST OF TABLES

Chapter 1 Introduction

Nowadays, in the face of more and more the stringent emission targets, every combustion passenger cars have the turbocharger engine version. At the same engine displacement, the engine equipped with a turbocharger can have the higher engine power than the engine without the turbocharger. With the same engine power, the turbocharger engine displacement can be smaller than the naturally aspirated engines, it means turbocharger would decrease the exhaust pollution. The increasing power of the engine is made by the highly compressed air, which comes from the turbocharger compressor part. A turbocharger is a turbine driven compressor. The hot exhaust air from the engine drives the turbocharger turbine. The turbine transfers the torque to the compressor through a shaft. So the turbocharger would not reduce the engine power for it is not directly connecting to the engine inside the components. The diesel engine used the turbocharger technology for a long period. To solve the compressor associated with surge unstable phenomena, the medium and large size turbocharger compressor used the RCT(recirculation casing treatment) also called ported shroud technology in a diesel engine. The RCT can decrease the vortex at the impeller part when the compressor is operated in the low mass flow rate working fluid. Due to the casting limitation, the small size compressor which the pressure ratio range from 1.2 to 2.5 is not easy to adopt the RCT technology. The 3D printer technology has been developing very quickly nowadays. It can also

be used for the future compressor production. Recently, the turbocharger has been installed to the gasoline engine to increase the engine power and decrease the emission pollution. Most gasoline engine displacement is from 1.3L to 2.0L. Hence, it is essential to investigate the flow and performance of the small-sized gasoline engine turbocharger RCT compressor by using the CFD technology.

1.1 Turbocharger for gasoline engine

The turbocharger first is most used in the diesel engines. Diesel as a fuel is not as combustible as gasoline. The air-fuel mixture in the cylinder should be under high pressure to effectively burn diesel. To withstand higher combustion pressures, diesel engines are manufactured with rugged, heavy-duty components. The heavier parts of a diesel engine cannot rotate at higher speeds. Less speed means less air goes into the combustion chamber. As a result, turbochargers help diesel engines draw more air into the combustion chamber. Gasoline is more flammable than diesel, so it burns at lower pressure. This means lower cylinder pressure and lighter moving parts that can rotate at higher speeds. This explains why the RPM band of gasoline engines is much higher than that of diesel engines. The higher the speed, the easier it is to inhale more air-fuel mixture during the intake stroke. This explains why diesel engines use turbochargers more than gasoline

engines. In addition, the role of turbochargers and gasoline engines is to increase the pressurization pressure (the ratio of the pressure at the outlet of the turbocharger compressor to the pressure at the inlet). In diesel engines, the role of turbochargers is to absorb more air. In addition to the strength of the engine components, there is virtually no limit to how much turbochargers can be added to a diesel engine. Most diesel engines are very robust compared to gasoline engines, so it can use them in large quantities. On the other hand, gasoline engines are limited by early ignition, which can damage the engine, so it cannot use as much pressurization as possible, and it must take special measures to avoid engine damage. Gasoline engines use spark ignition, the gasoline is much more combustible that it can ignite much easier, but if the pressure is too high during compression, the air-fuel mixture will ignite too quickly during the compression phase prior to spark plug ignition, and the impact will damage the engine. There are several ways to avoid this, such as using knock sensors that, when they detect a knock, back up the pressure and reduce the engine's compression ratio which reduces fuel economy. Depend on the ECU development, the gasoline engine can be controlled precisely to avoid the high pressure inside the engine. The inherent disadvantage of a diesel engine is that it is difficult to draw enough air flow into the combustion chamber, and turbocharge can help the diesel engine to fight this situation. For commercial diesel engines, the goal is to increase the flow to the engine, not the combustion pressure. This means that the overall "bost" provided by turbocharger using

commercial diesel engines has traditionally been very low. In practice, this means that diesel turbochargers are usually larger than gasoline counterparts, have large turbine sections, can handle large amounts of exhaust gas, and need to provide enough intake to keep the cylinders full. For gasoline engines, the purpose of increasing turbochargers is to increase engine power, so the goal is to increase the pressure in the combustion chamber. This means gasoline turbochargers tend to be smaller and are designed to operate at higher RPM, providing higher pressure increases without significantly increasing airflow. In addition, because gasoline engines need to run at a wider RPM range, it is important that gasoline turbochargers accelerate faster than diesel engines. A final point about gasoline engines is that increasing engine and turbocharger speeds generate a lot of heat and require proper management that turbines use the back pressure of these hot gases to improve efficiency and performance. Figure 1 shows the turbocharger conponents and their funtions.

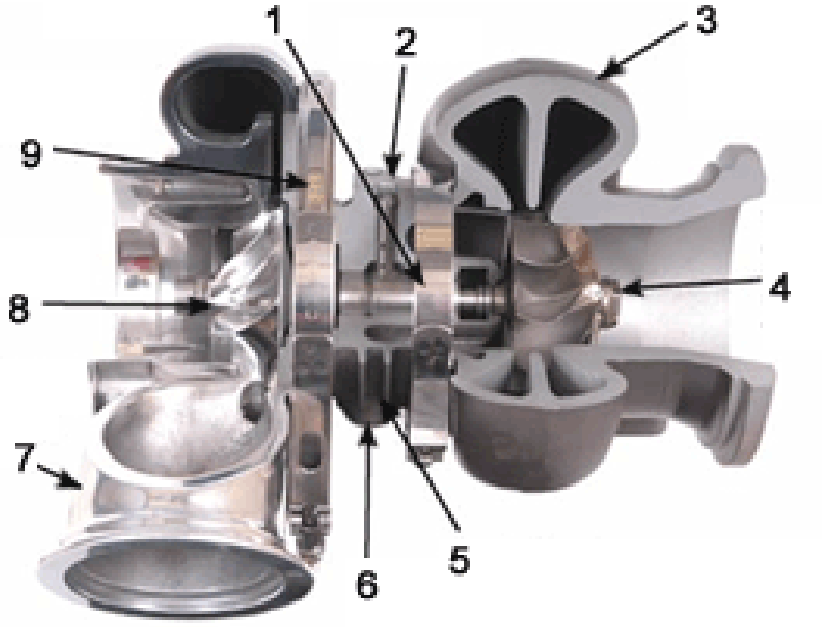

1	Ball bearings (support and control the rotating group)
2	Oil inlet
3	Turbine Housing (collects exhaust gases from the engine and directs it to the turbine wheel)
4	Turbine Wheel (converts exhaust energy into shaft power to drive the compressor)
5	Center Housing (supports the rotating group)
6	Oil outlet

7	Compressor Housing (collects compressed air and directs it to the engine)
8	Compressor wheel (pumps air into the engine)
9	Backplate (supports the compressor housing provides aero surface)

Fig.1 Automobile turbocharger components and functions

1.1.1 Compressor

The compressor is made up of impeller, diffuser and volute housing. Figure 2 shows the geometry of the turbocharger compressor. The process of compressor work was shown in Figure 3. Firstly, the air is drawn into the compressor and the energy is provided to the compressor wheel by the turbine, via the rotating shaft. Secondly, the spinning wheel passes this energy to the air by increasing its velocity and increasing its temperature and pressure. Thirdly, the diffuser slows the air down, converting the kinetic energy to increase the pressure further. Lastly, the volute continues to diffuse the air, collection it and directing it to the outlet.

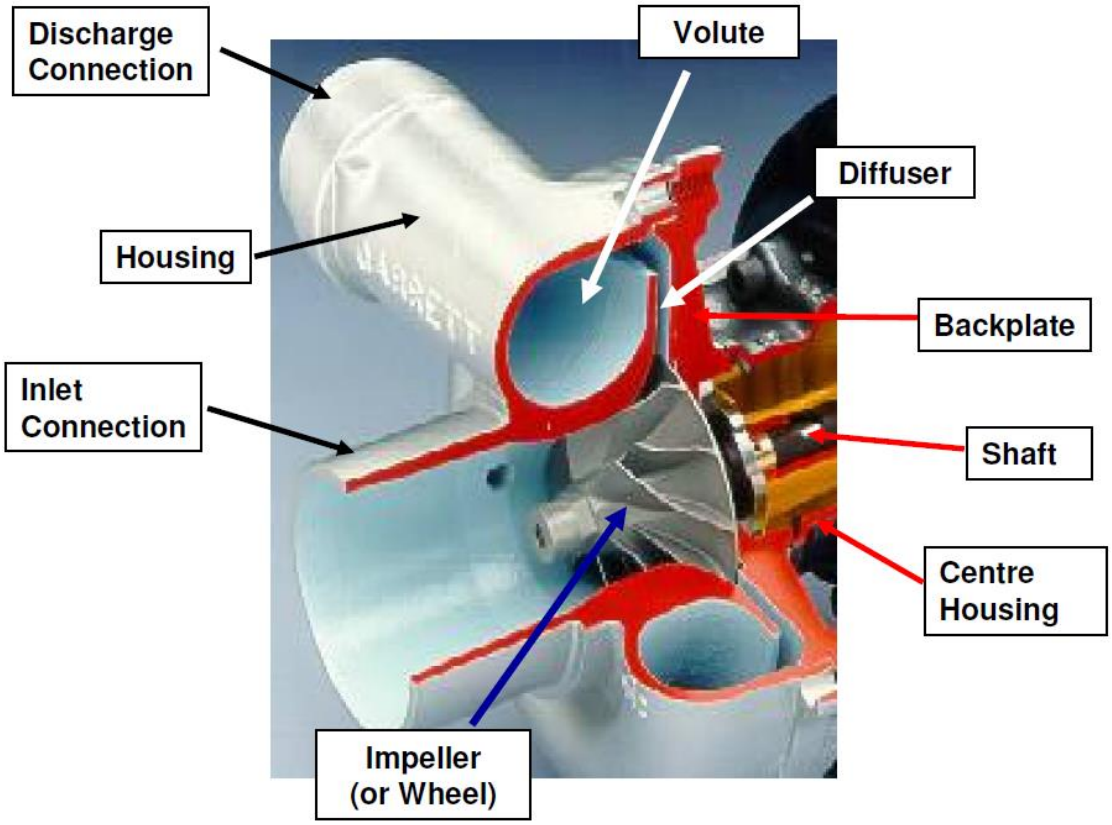

Fig.2 Automobile turbocharger compressor and components

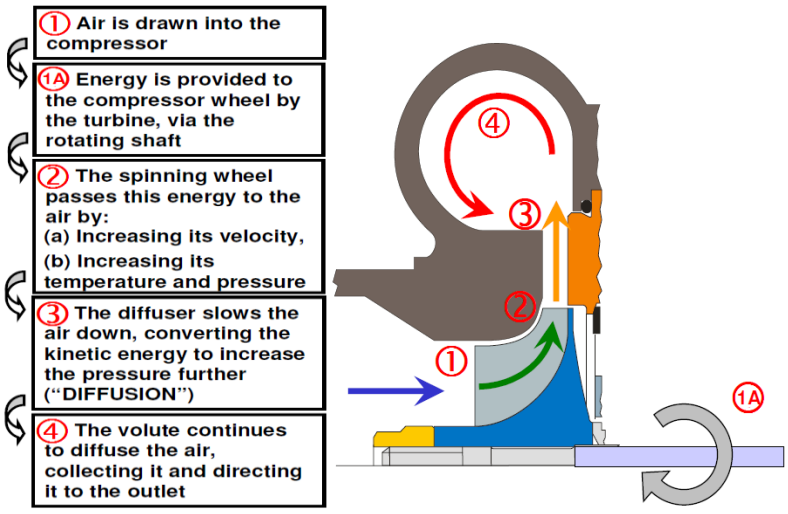

Fig. 3 The process of compressor work

1.1.3 Turbine

Turbocharger turbines work in very harsh environments. The turbine is made of exhaust gas that can exceed 1025℃ and is very corrosive. The exhaust valve also encounters the same corrosive, high-temperature gases, but the exhaust valves do not approach the peak temperature of the exhaust because they discharge a large amount of heat into the coolant through the seat and stem. The exhaust valve in the competing engine is at least half of the time on the seat which about two-thirds of the production engine is on the seat. The valve continuously transfers heat to the guide through the valve stem, and when the valve is in place, the heat is quickly transferred to the cylinder head through the valve seat. These cooling paths make the temperature of the exhaust valve much lower than the EGTs. However, the turbine wheel lives in a continuous high-speed jet consisting of these gases. Although the turbine nozzle has an expansion phenomenon, some of the gas is cooled, and the temperature at the top of the turbine rotor can be close to the exhaust temperature. In addition, many turbocharger rotor systems operate well above 100,000 rpm, some close to 150,000 rpm. This exerts a huge pulling force, as well as bending and vibration loads, from the centrifugal force. This environment requires the use of nickel-base superalloys for turbine wheels. These alloys retain high strength values at this elevated temperature. The newly produced turbines are suitable for continuous operation at an exhaust gas turbocharger with an inlet temperature of 950 ℃. Production turbines are typically cast by Inconel

713C or 713LC. The turbine casting is subjected to hot isostatic pressing to improve its structure and then heat treated to the required strength level. The turbine is shown in Figure 4.

Fig.4 Automobile turbocharger Turbine

Chapter 2 Turbocharger Compressor

A turbocharger compressor is composed of the inlet duct, compressor, impeller diffuser, and volute.

2.1 Inlet Duct

The purpose of the inlet part is to direct the ambient air flow to the impeller of the compressor. There are two basic forms of the inlet duct, an axial inlet duct, and radial inlet duct. The most medium and small size turbocharger compressor use the axial inlet duct. Some small displacement cars engine room is very narrow, in this case, the radial inlet duct would be used for the turbocharger compressor. Figure 5 shows the compressor axial and radial inlet duct turbocharger.

axial inlet duct radial inlet duct

Fig.5 Automobile turbocharger compressor axial and radial inlet duct

2.2 Impeller

The first requirement of the impeller is to draw the approaching air into the blade passage as smoothly as possible. In order to do this, the blades must be properly aligned with the incident velocity vector. In the axial or near-axial direction, the flow approaches the impeller at an absolute speed C_1, and the blades rotate at a local velocity U_1 as shown in Figure 6. The velocity of the relative velocity vector on the blade is critical for efficient and stable operation. The angle of incidence is the difference between the blade and the flow angle, which should not exceed several orders of magnitude for high performance.

$$\mathrm{i} = \beta_{1\mathrm{b}} - \beta_1 \tag{1}$$

After entering the vane passage, the airflow diffuses through the impeller and exits at the speed and direction controlled by the impeller blades. The degree of sweeping has an important influence on the operation. Figure 7 is a comparison of the exit velocity of the non-swept impeller and the swept-back impeller: In the former case, as shown in the upper left diagram, the flow exits at a relative speed W_2 in the radial direction. In addition to the blade speed U_2, an absolute speed C_2 is obtained, which forms the inlet speed of the stationary component downstream of the impeller. In the latter case, the upper right corner and the graph show that W_2 tends to rotate in the direction, the flow angle β_2 is negative, and C_2 is correspondingly smaller.

Figure 7 also shows the difference in flow regimes for high and low flow conditions. The meridian component of the flow control speed C_{m2}. Considering the upper left and lower left diagrams of the non-swept impeller, the relative velocity W_2 moves along the radial direction of the blade, which is consistent with C_{m2}. Therefore, it follows the change in flow, but it is still in the radial direction. The absolute speed C_2 also changes, but its tangential component $C_{\theta 2}$ remains the same because the blade speed U_2 is constant. The two figures in the upper right and lower right corners show the corresponding conditions for the sweeping impeller outlet at high flow rates and low flow rates. In this case, W_2 is no longer aligned with C_{m2}. C_{m2} increases in size with mass flow, W_2 but still follows the direction of the blade, as U_2 remains unchanged and $C_{\theta 2}$ is now reduced. The sweeping impeller is an almost universal choice for turbocharger compressors. The wide range of compressor maps is very important and can be used with sweepback angles of up to 40-50 degrees.

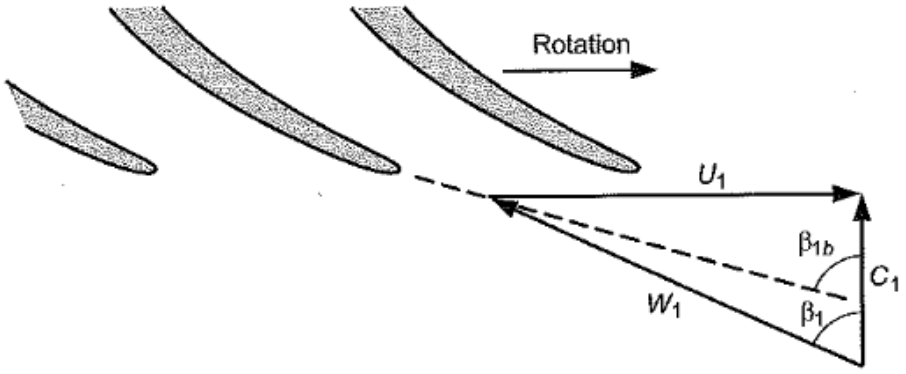

Fig. 6 Impeller inlet velocities

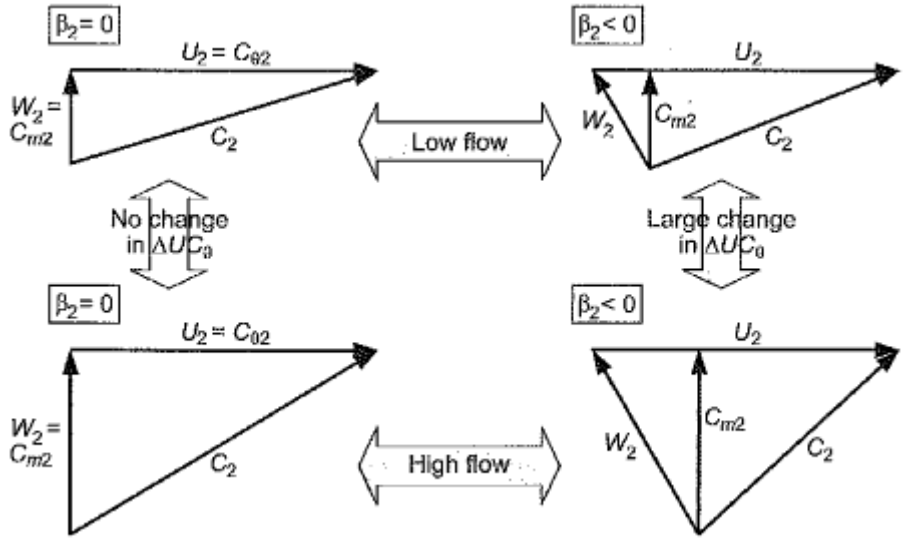

Fig. 7 Impeller exit velocities for non-backswept and backswept impellers and high flow rate.

2.3 Diffuser

Checking the flow away from the impeller outlet indicates that the absolute velocity is usually very high. In fact, the impeller outlet kinetic energy usually accounts for 30-50% of the axial work input to the compressor stage, and in order to improve the energy, it is important to recover as much as possible. This is the function of the diffuser that follows the impeller. A diffuser can have one of several configurations. For small compressors, the simplest and probably the most common is the vaneless diffuser. As with all diffusers, a bladeless diffuser needs to increase the area in the flow direction to slow down the flow, and this is provided naturally by increasing the

radius as the flow moves outward. As the flow diffuses, the density increases and the flow rotate tangentially. In practice, friction acting on the boundary layer also impeded the flow close to the end wall, and if sufficient diffusion was allowed, the radial motion in the end wall flow could be completely stopped and the flow would move inward toward the impeller, thus establishing recycling in the diffuser. In a limited space, a simple vaneless diffuser may actually be better than a highly damaged channel diffuser.

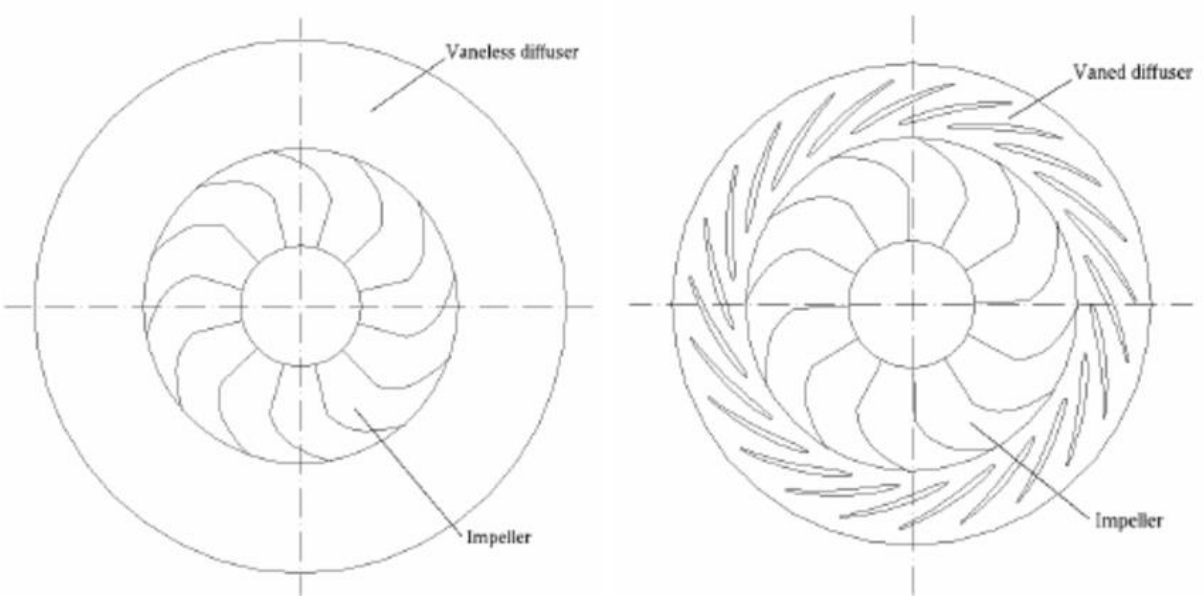

Fig.8 Vaneless and Vaned diffuser flow

2.4 Volute

The volute is a spiral casing that collects air from the diffuser and continues to diffuse and transfer it to the pipe that connects the intercooler or the intake manifold. Fluid kinetic energy is converted to thermodynamic energy, which increases the temperature and pressure of the fluid. The cross-section of the volute is usually cantilevered to limit the radial space requirements and allow it to enter the rear surface of the compressor where there is usually a flange or clamp that connects the compressor to the bearing housing or turbine Pressure on the structure. In order to improve the performance of the compressor, the volute flow has been studied. In recent years, in the research of the volute, the loss mechanism has been an effective means to improve the performance of the volute. The volute cannot recover the radial velocity at the diffuser outlet, and the radial component of the velocity becomes the eddy component in the volute. Since the eddy current velocity component in the volute is the main cause of the compressor performance degradation, reducing the eddy current loss can improve the performance of the compressor.

.

Fig. 9 Compressor Volute

2.5 Recirculation Casing Treatment

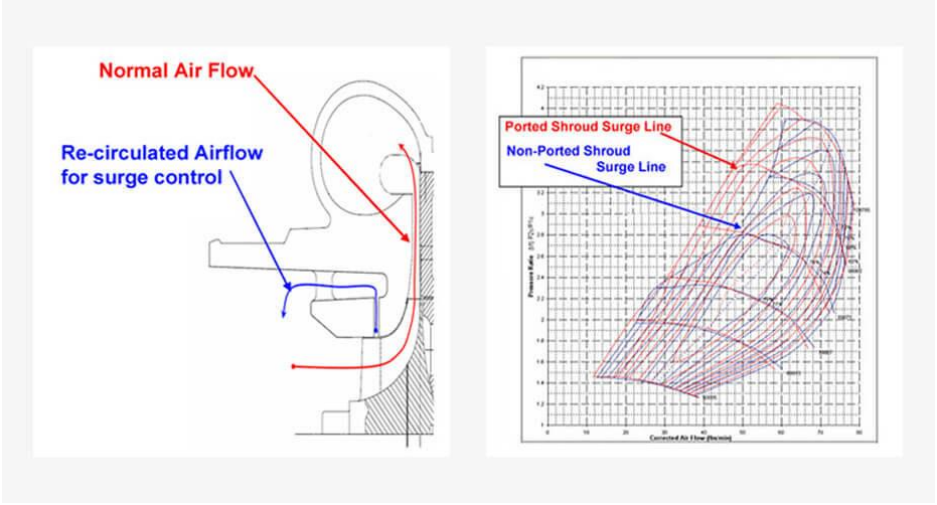

Fig. 10 The RCT concept and compressor map

The recirculation casing treatment (RCT) also called the ported shroud in Industry. A recirculation casing treatment compressor is a feature that is

incorporated into the compressor casing. Its function is to move the surge line further to the left in Figure 10, allowing some airflow to leave the wheel through the port to prevent surge. This provides an additional range of use and allows a larger compressor to be used for higher flow requirements without the risk of running the compressor to a dangerous surge condition. The presence of recirculation treatment typically has less impact on compressor efficiency.

2.6 Compressor Map

Figure 11 shows a typical compressor map. The compressor map is a graph depicting the performance characteristics of a particular compressor, including efficiency, mass flow range, pressure ratio, and turbine speed. The pressure ratio is defined as the absolute pressure of the outlet divided by the absolute pressure of the inlet. The gauge pressure is measured above atmospheric pressure, so the gauge pressure reading under atmospheric conditions will be zero. The boost meter measures the manifold pressure relative to atmospheric pressure and is, therefore, the gauge pressure. Mass flow is the mass of air passing through the compressor and engine at a given time, usually expressed as kg/s. Mass flow can be measured physically, but in many cases, it is sufficient to estimate the mass flow in order to select the right turbine. The surge line is the left side boundary of the compressor map.

The operation to the left of this line represents a flow unstable area. This area is characterized by a slight flutter to the violent fluctuation of the boost and the "howling" of the compressor. When one of two conditions exists, the most common is a surge. The first and most destructive is the surge under load. Surge usually occurs when the throttle closes quickly after being pressurized. A transplanted crown compressor is a feature that is incorporated into the compressor casing. Its function is to move the surge line further to the left, allowing some airflow to flow out of the wheel through the port to prevent surge. The choke line is the right edge of the compressor map. For Garrett maps, the chock line is usually defined by points that are less than 58% efficient. In addition to the rapid decline in compressor efficiency beyond this, the turbine speed will also approach or exceed the allowable limit. The turbo speed line is a straight line with constant turbo speed. The turbo speed at the point between these lines can be estimated by interpolation. As the turbo speed increases, the pressure ratio and mass flow rate increases. As shown in the throttle line description above, the turbo speed line is very close to the far right of the map. Once the compressor has exceeded the throttling limit, the turbo speed will increase rapidly and it is likely that the turbine will over speed. The efficiency island is a concentric area on the map that represents the efficiency of the compressor at any point on the map. The smallest island near the center of the map is the most efficient or highest island. As the ring is removed from there, the efficiency drops by the indicated amount until the surge and chock

limits are reached.

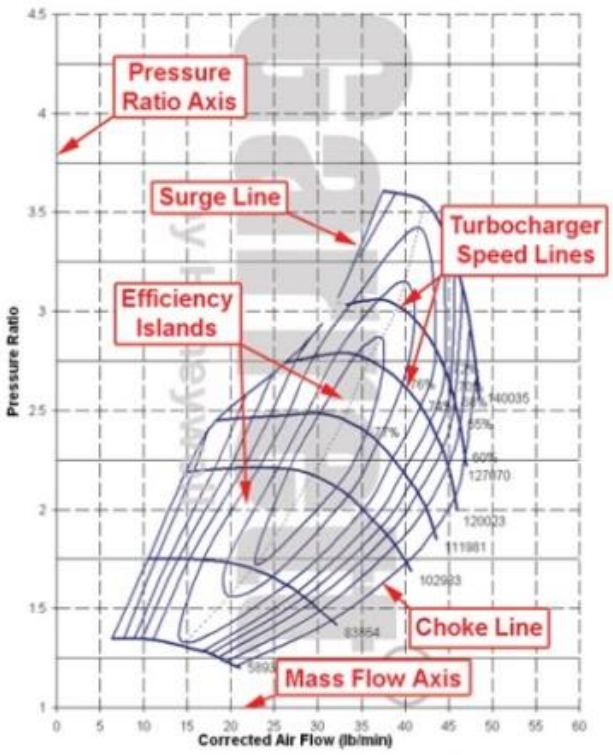

Fig. 11 A typical compressor map

2.7 Unstable Condition of Turbocharger Compressor

2.7.1 Surge margin

Axisymmetric stall, commonly known as compressor surge; pressure surge is the complete compression caused by the inability of the compressor to continue to withstand the compressed air that has been compressed in the future and the violent discharge of previously compressed air from the

engine intake. malfunction. The compressor either experiences more than its pressure rise limit or is subjected to excessive loads so that it cannot absorb transient disturbances, resulting in a rotational stall that can propagate throughout the compression in less than a second. machine. Once the engine pressure ratio is reduced to the level at which the compressor can maintain a steady flow, the compressor will return to normal flow. However, if the conditions that cause the stall still exist, the return of the steady airflow will reproduce the conditions at the time of the surge, and this process will be repeated. This “lock-up” or self-resetting stall is particularly dangerous, and the vibration level is very high, causing accelerated wear and possible damage to the engine, and even destroying the engine completely through the breakage of the compressor and stator blades and their subsequent intake, damaging the engine downstream. component. In CFD simulations, there is no clear definition to guarantee the time of the surge. The surge line point herein is defined as compressor efficiency equal to 60%.

2.7.2 Chock margin

Compressor chock is an abnormal condition of a centrifugal compressor. The centrifugal compressor is chocked when operating under low discharge pressure and high flow conditions. These high flows at the chock point of the compressor are actually the maximum flow that the compressor can pass.

Any further reduction in the exit resistance will not result in an increase in compressor output. This condition is also called the stalling of the centrifugal compressor. When the flow resistance in the compressor discharge line is significantly lower than the normal level, the stone wall or chock point of the centrifugal compressor will appear. Due to the low resistance, the back pressure of the compressor discharge is very low. According to the fixed RPM value given by the compressor map, as the compressor exhaust back pressure drops, the compressor output increases. This leads to an increase in the gas velocity in the centrifugal compressor. An increase in gas velocity can occur until it reaches its maximum at sonic speed. When the gas velocity of any part of the compressor is close to the speed of sound, it is called the chock or stone wall of the compressor operation. At the throttling point, the gas velocity and gas flow cannot exceed this value.

Chapter 3 CFD simulation of Non-RCT turbocharger compressor

3.1 CFD technology for turbomachinery

Until a few decades ago, the only way for auto companies to test product quality, especially engine performance, was to conduct experimental tests. It is well known that it takes time to conduct an experiment and requires a long post-processing phase in order to analyze the correctness of the initial assumptions and verify the results obtained. Computational Fluid Dynamics (CFD) is a branch of fluid mechanics that uses numerical analysis and data structures to solve and analyze problems involving fluid flow and to perform the calculations required to simulate the interaction of liquids and gases with surface conditions defined by boundary conditions. High-speed supercomputers can provide better solutions. Ongoing research has developed software that improves the accuracy and speed of complex simulation scenarios such as transonic or turbulent flow. The basic basis for almost all CFD problems is the Navier-Stokes equation, which defines many single-phase (gas or liquid, but not both) fluid flows. These equations can be simplified by removing the term describing the viscous effect, resulting in the Euler equation. Further simplification, by removing the term describing the vorticity, a complete potential equation can be obtained. Finally, for small perturbations in subsonic and supersonic (non-transonic or

hypersonic), these equations can be linearized to obtain a linearized potential equation. This paper uses ANSYS CFX for CFD simulation. This CFD package was chosen because it is suitable for modeling the mechanical flow of the impeller and can easily handle the rotating area. The entire process, from the definition of geometry to the post-processing of data, can be managed directly from ANSYS Workbench. In particular, the parameter setting window of ANSYS Workbench allows you to set up all simulations by easily changing the boundary conditions: this tool is especially useful when running steady-state simulations for calculating compressor maps.

Fig. 12 CFX simulation process

3.2 Flow equations and models

Fluid mechanics is the discipline that describes fluid flow. The macroscopic behavior of a fluid is described by a set of nonlinear partial differential equations that allow the evaluation of important flow variables such as pressure, temperature, density, and velocity throughout the field. Because fluid dynamics problems often have complex, highly nonlinear phenomena, they are highly complex. It should also be remembered that there are currently no analytical solutions for full Navier-Stokes. The birth of

computational fluid dynamics (CFD) has made it possible to study flows in complex three-dimensional geometries with high complexity. CFD involves solving discrete forms of governing equations with the help of a supercomputer. However, computing resources are limited: therefore, in order to reduce the number of variables and computation time required for the calculation, it is always necessary to make assumptions about the flow. Once the initial conditions and boundary conditions are determined, the evolution of the fluid is derived using the governing equations. These are mass conservation, momentum balance, and energy balance. These equations can be written in integral form or in differential form. The integral formula is defined in the control volume. The control volume is an area that appears to the outside observer to be fixed in size and shape in space. In other words, it can be thought of as a spatial region surrounded by an invisible, rigid, massless surface called the control surface. Mass, energy, and heat can be exchanged through the control surface. By reducing the size of the control volume, the differential formula can be obtained directly from the integral formula to reach the size of infinitesimal fluid particles.

$$\frac{\partial \rho}{\partial t} + \frac{\partial}{\partial_{x_i}}(\rho u_i) \tag{2}$$

$$\frac{\partial(\rho u_i)}{\partial t} + \frac{\partial(u_i u_j)}{\partial x_i} = -\frac{\partial p}{\partial x_i} + \frac{\partial \sigma_{ij}}{\partial x_j} + \rho f_i \tag{3}$$

$$\frac{\partial(\rho e^0)}{\partial t} + \frac{\partial(u_i e^0)}{\partial x_i} = -\frac{\partial(p u_i)}{\partial x_i} - \frac{\partial q_i}{\partial x_j} + \frac{\partial(u_i \sigma_{ij})}{\partial x_i} \tag{4}$$

Where i, j =1,2,3 are the indices of the Cartesian coordinates,

u_i, u_j = velocity components,

σ_{ij} = stress tensor,

f_i = external force,

e^0 = e +1/2$u_i u_j$ = specific total energy,

e = specific inner energy,

q_i= heat flux.

The first equation describes mass conservation, the second equation describes momentum balance, and the third equation describes total energy balance. The second term is the advection term: it is highly non-linear and describes the force exerted by other surrounding fluid particles on the fluid particles.

Turbulence involves unsteady changes in flow variables, such as random changes in velocity over time. In order to facilitate the study of this complex flow, the Reynolds number can be introduced for decomposition.

$$\frac{\partial \bar{\rho}}{\partial t} + \frac{\partial}{\partial x_i}(\bar{\rho}\bar{u_\iota}) = 0 \quad (5)$$

$$\frac{\partial(\overline{\rho u_\iota})}{\partial t} + \frac{\partial(\overline{\rho u_\iota u_j})}{\partial x_j} = -\frac{\partial \bar{p}}{\partial x_i} + \frac{\partial \bar{\sigma}_{ij}}{\partial x_j} + \frac{\partial \tau_{ij}}{\partial x_j} \quad (6)$$

$$\frac{\partial}{\partial t}\left(\bar{\rho}\left(\tilde{e}+\frac{\tilde{u}_i\tilde{u}_j}{2}\right)+\frac{\overline{\rho u_i'' u_i''}}{2}\right)+\frac{\partial}{\partial x_j}\left(\bar{\rho}\tilde{u}_j\left(\tilde{h}+\frac{\tilde{u}_i\tilde{u}_i}{2}+\tilde{u}_j\frac{\overline{\rho u_i'' u_i''}}{2}\right)\right)=$$

$$\frac{\partial}{\partial x_j}\left(\tilde{u}_i\left(\tilde{\sigma}_{ij}-\overline{\rho u_i'' u_i''}\right)\right)+\frac{\partial}{\partial x_j}\left(-\bar{q}_j-\overline{\rho u_i'' h''}+\overline{\sigma_{ij} u_i''}-\overline{\rho u_j''\frac{u_i'' u_j''}{2}}\right) \qquad (7)$$

The Reynolds Averaged Navier-Stokes equations(RANS) is the averaged version of the momentum equations. The new factor τ_{ij} defined as follows:

$$\tau_{ij}=-\overline{\rho u_i'' u_j''} \qquad (8)$$

This expression is called the Reynolds stress tensor: it consists of a symmetric matrix defined by six independent components that explain the macroscopic transport of momentum at the turbulent scale. The Reynolds stress tensor introduces six new unknowns for this problem: therefore, a modeling strategy should be used to close the equations.

Of all available eddy viscosity models for solving the RANS equation, the most common one is to solve two transport equations for calculating turbulence. Among them, the K−ω turbulence model, the first development of Wilcox, represents one of the most commonly used turbulence models in industrial research today. In principle, the turbulent model passes the transfer equation flow energy $K=\frac{u_i u_i}{2}$ and a specific dissipation rate ω. K-ω model takes the following form:

$$\left(\frac{\partial}{\partial t}+\overline{u_i}\frac{\partial}{\partial x_i}\right)\mathrm{K}=\mathrm{P}-C_\mu K_\omega+\frac{\partial}{\partial x_j}\left[\left(\vartheta+\frac{\vartheta\tau}{\sigma_K}\right)\frac{\partial K}{\partial x_j}\right]$$

$$\left(\frac{\partial}{\partial t}+\bar{\mu_{\iota}}\frac{\partial}{\partial x_j}\right)\omega=\left((C_{\varepsilon 1}-1)\frac{\omega}{K}\right)\mathrm{P}-(C_{\omega 2}-1)C_{\mu}\omega^2+\frac{\partial}{\partial x_j}\left[\left(\vartheta+\frac{\vartheta\tau}{\sigma_{\omega}}\right)\frac{\partial\omega}{\partial x_j}\right] \tag{9}$$

where C_{μ} , σ_K , $C_{\varepsilon 1}$ and $C_{\omega 2}$ are modelling calibrated experimental coefficients. Turbulent viscosity defined as $\nu\,\vartheta\tau = \mathrm{K}/\omega$, the production of turbulent kinetic energy P and specific dissipation rate ω are defined as follows:

$$\mathrm{P}=-\overline{u_{\iota}'u_j'}\frac{\partial\overline{u_{\iota}}}{\partial x_j}=2\vartheta_T S_{ij}S_{ij} \tag{10}$$

$$\omega=\frac{\vartheta\overline{\partial u_{\iota}'\partial u_{\iota}'}}{C_{\mu}K\partial x_j\partial x_j} \tag{11}$$

Compared to the other two equations turbulence models such as k-t extinction, the K-ω model has some advantages. First, it better predicts boundary layer flow with pressure gradients. In addition, the k-t mass extinction equation becomes singular on the wall rather than the area that is very close to the wall, unless the expensive low-Re formula is calculated, the K-ω can also be integrated into the small grid spacing on the wall. The main problem with this method is the treatment of the interface, especially the boundary layer edge, resulting in a non-physical sensitivity to the free flow value K-ω. In addition, there is no good prediction of the separation starting point and separation amount under the reverse pressure gradient. To solve these problems, the Shear-Stress-Transport (SST) K-ω model has been improved to correct the defective standard K-ω model by increasing the

conditions of cross-diffusion and producing a formulation that uses eddy viscosity. In addition, the SST formula allows switching to the K-t equation in free flow: in fact, the latter is less sensitive to the characteristics of the inlet free-flow turbulence; the K-ω model is not used to solve the boundary layer.

3.3 Non-RCT compressor geometry

In this thesis, the BorgWarner company K04 compressor is chosen for the basic research model. This compressor is used for the 1.3-1.6L gasoline engine and without the RCT casing.

Fig. 13 BorgWarner company K04 turbocharger

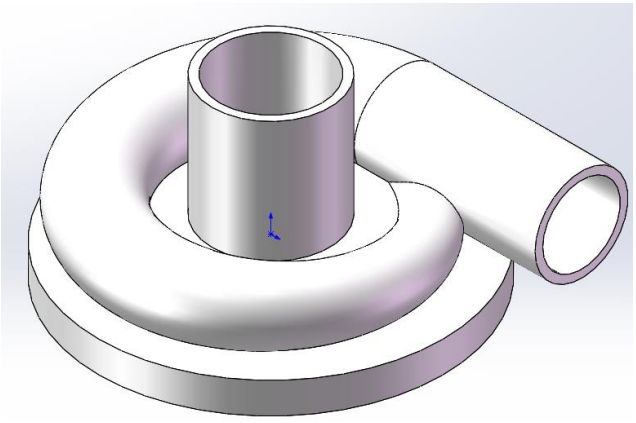

Fig. 14 Basic non-RCT compressor casing

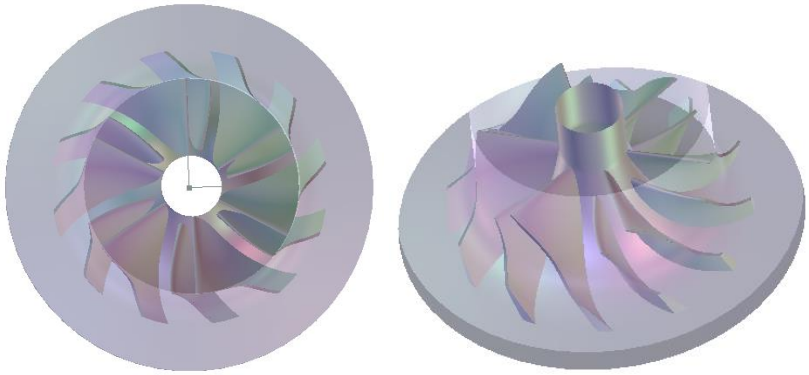

Fig. 15 The impeller of this non-RCT compressor

Figure 14 shows the basic non-RCT compressor casing. This compressor is made by Solid Works. For CFD simulation, this model modified from the K04 compressor. The impeller of this non-RCT compressor is shown as Figure 15. The ANSYS blade-gen is the tool that making this impeller. The compressor casing inlet duct diameter is the same with the K04 compressor. For the limited of 3D printer, the outlet duct diameter is the constant diameter pipe which is different from the real K04 compressor that is outlet duct is linear increase the diameter. For the volute design, the area of each volute section is a linear increase. The equation is

$$A_\theta = 1.907\theta + 20 \quad (\theta = 0^\circ \sim 360)^\circ \tag{12}$$

The design of impeller is also base on the K04 compressor impeller. Input the K04 compressor map data to the ANSYS CCD (centrifugal compressor design) tool, the software automatic exports the data of impeller. Putting this data into the ANSYS Blade-gen tool, the geometry of the impeller automatic

generates. The geometrical configuration of the compressor of this non-RCT compressor is shown as Figure 16. The fluid domain of compressor is shown at Figure 17. Table 1 shows the compressor geometry parameters.

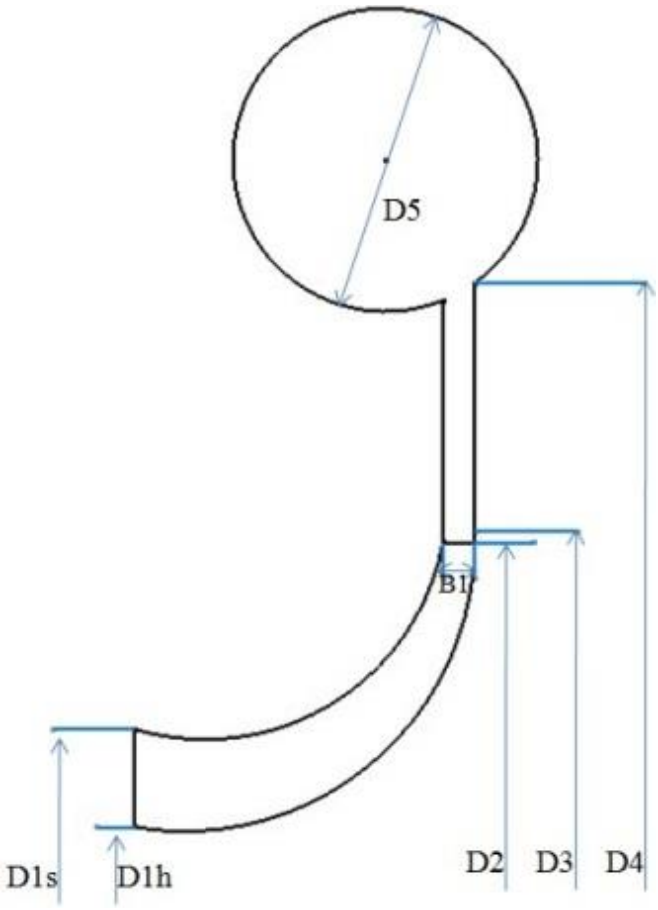

Fig. 16 The geometrical configuration of the compressor

Table 1 Compressor geometry parameters

Impeller main blade number	6
Impeller split blade number	6
Impeller inlet hub diameter(D1h)	10.3mm
Impeller inlet shroud diameter(D1s)	36.28mm
Impeller outlet diameter(D2)	46mm
Vane-less diffuser inlet diameter(D3)	61.8mm
Vane-less diffuser outlet diameter(D4)	86mm
Vane-less diffuser width(B1)	4mm
Volute outlet diameter(D5)	30mm

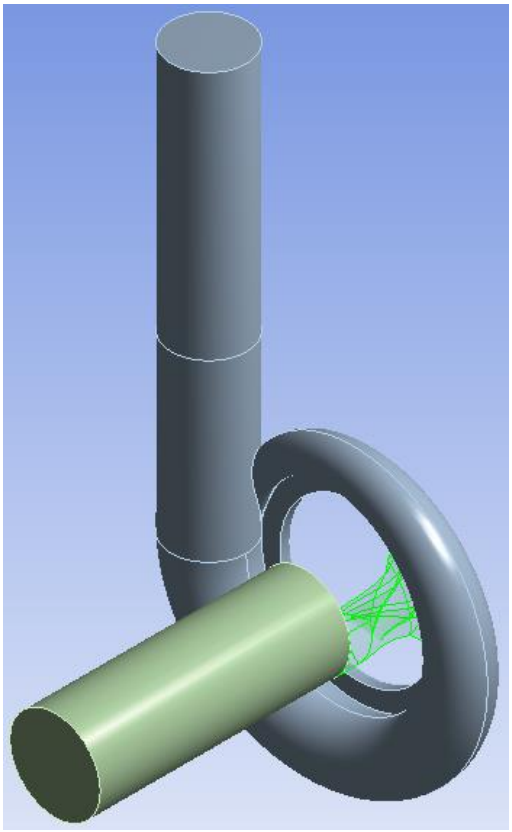

Fig. 17 The fluid domain of Non-RCT compressor

3.4 Meshing generation and Independence

The compressor casing, inlet, and outlet part mesh are generated by the ANSYS mesh tool. The turbo-grid is the tool which makes the impeller part mesh. All mesh type is a hexagon. The ANSYS mesh tool has three types of mesh relevance center: Coarse, Medium and Fine. Each type can set the different size of mesh grid. In this study, for the mesh grid independence test, there are five sizes of mesh were generated. The relevance center type and a number of each text mesh grid group are shown in Table 2. Using the compressor pressure ratio and efficiency data to check the mesh independent in different mass flow rate at the 140,000 RPM, as shown in Figure 18 and Figure 19, the Fine type mesh which grid mesh number is 933988 the simulation results become constant. The number of one impeller blade mesh is 738,688. And volute, inlet, and outlet part number is 195,300. Total mesh number is 933,988. The calculation time for one model was 6 hours by using the 8 cores PC. The mesh is shown in Figure 20 and Figure 21.

Table 2 Mesh relevance center type and grid number

Relevance Center type	Coarse	Medium	Fine	Fine	Fine
Mesh Grid Number	338831	581550	933988	1023011	1305278

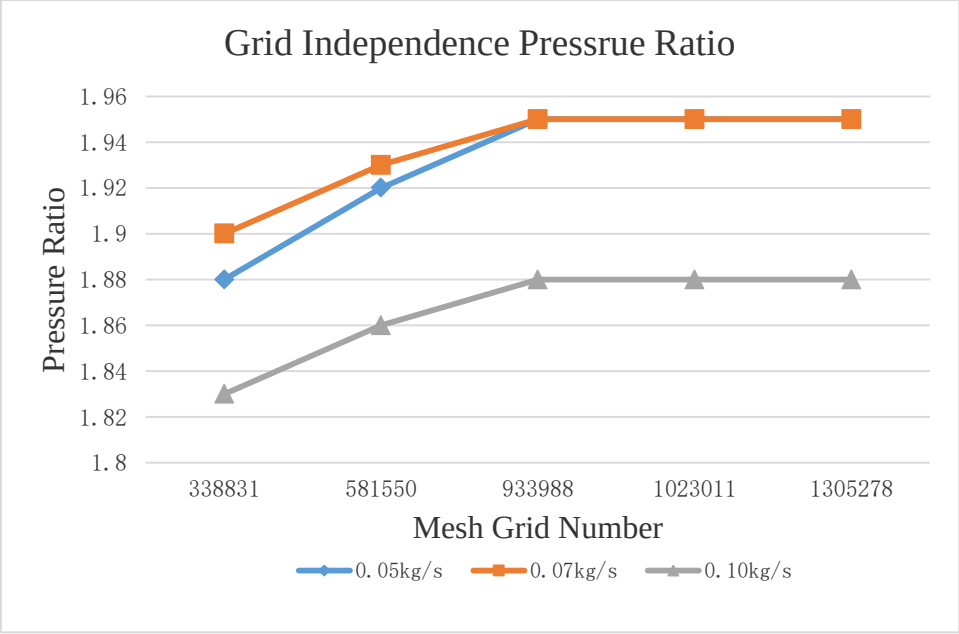

Fig. 18 Grid independence test for the compressor pressure ratio

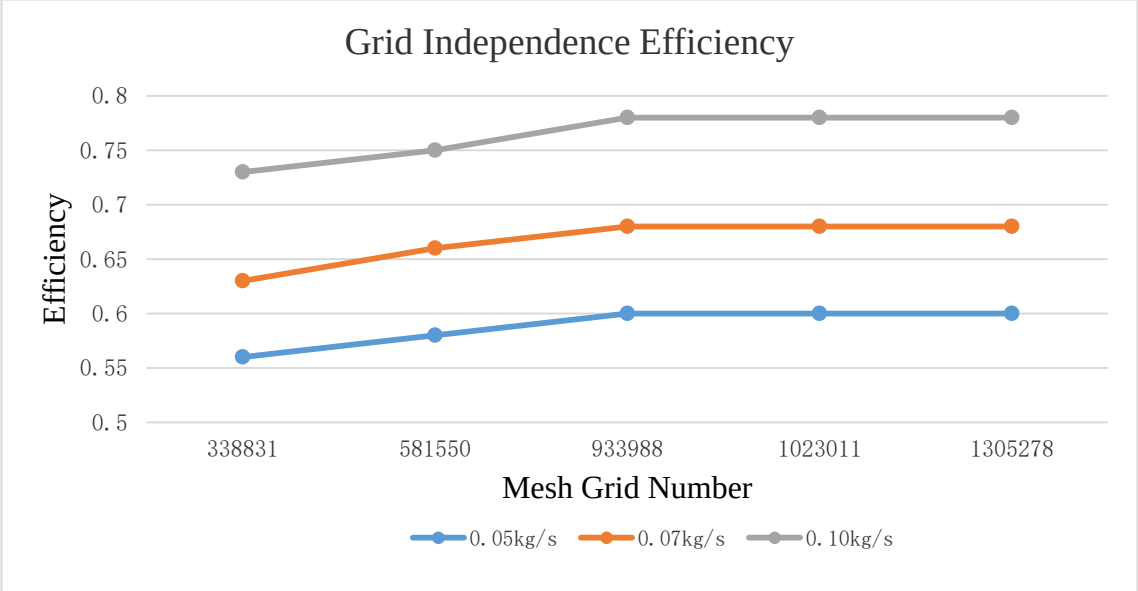

Fig. 19 Grid independence test for the compressor efficiency

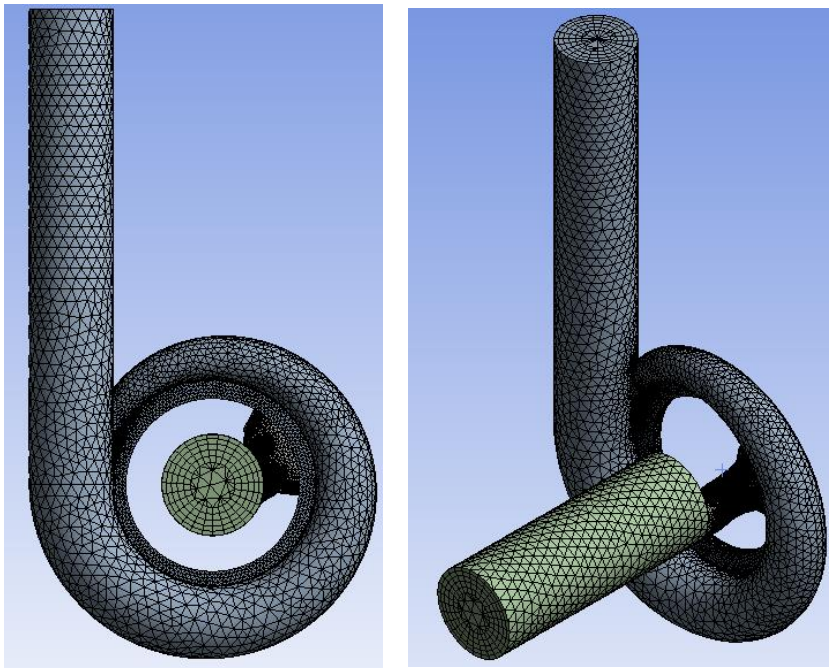

Fig. 20 Mesh of Non-RCT compressor

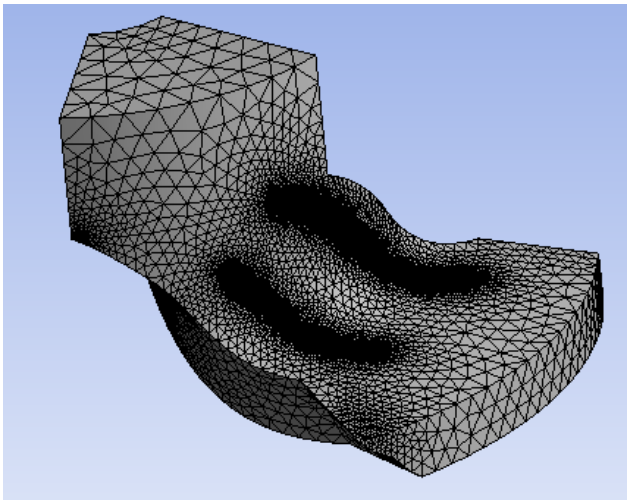

Fig. 21 Mesh of Non-RCT compressor one passage impeller

3.5 CFD simulation setting and validation

In this simulation, the whole operating range of the compressor is to simulate. There are six RPM for simulation: 60,000rpm, 80,000rpm, 100,000rpm, 120,000rpm, 140,000rpm and 160,000rpm. The working mass flow range is 0.01kg/s to 0.17kg/s. The turbulence model is a k-Ω-SST model. Frozen rotor plane is the interface type. Table 3 shows the CFD setting parameters. For validating the numerical results, the accuracy of numerical simulation results was verified by the compressor product company test data. Table 4 shows the company test data and the simulation data from this study simulation. There are four working mass flow rate points which at the same compressor rotating speed to check the error between the company data and simulation data. The simulation error is less than 1%.

Table 3 CFD setting parameters

Inlet total pressure	1 atm
Inlet total temperature	300k
Outlet mass flow rate	0.01kg/s ~0.17kg/s
Rotational speed rpm	60,000~180,000
Turbulence model	k-Ω-SST
Interface type	Frozen Rotor plane

Table 4 Company test data and the simulation data

Pressure Ratio at 140,000RPM				
Mass flow rate(kg/s)	0.08	0.09	0.1	0.11
Company data	1.93	1.91	1.89	1.86
CFD results	1.93	1.91	1.88	1.85
Efficiency at 140,000RPM				
Mass flow rate(kg/s)	0.08	0.09	0.1	0.11
Company data	0.73	0.76	0.78	0.8
CFD results	0.72	0.75	0.78	0.8

3.6 Simulation Results

First, the simulation results of 140,00RPM. To explain the flow field inside the compressor, there are four different mass flow rate points at 140,000rpm

would be chosen. The first and second points are the mass flow rate at 0.05kg/s and 0.075kg/s. These two points are near the surge area at this compressor rotating speed. The third point is the 0.10kg/s. At this point, the engine has the maxing power when the engine RPM is 3500. The fourth point is the 0.11kg/s, which is the highest efficiency point of this compressor. And Figure 22 shows the compressor volute cross-section angle distribution.

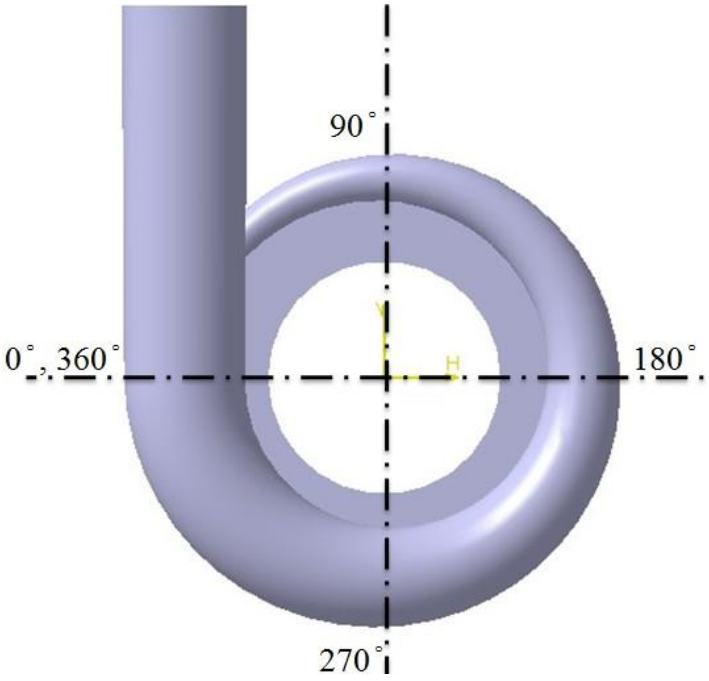

Fig. 22 Compressor volute cross-section angle distribution

3.6.1 Pressure distribution

3.6.1.1 Pressure distribution at mass flow rate equal to 0.05kg/s

This figure 23 shows the pressure distribution at 0.05kg/s the compressor. The surface of the volute does not have higher pressure. Each cross section of volute pressure is shown in figure 24. In this figure, the high pressure area only in the middle part inside the volute, it cannot spread the high pressure to the all volute surface. In this low mass flow rate, the kinetic energy does not totally transfer to the pressure potential energy. This is the reason that the low mass flow the efficiency is lower. One impeller passage at this mass flow rate pressure distribution is shown in figure 25. The whole part of this one impeller, the pressure is lower. It can increase the pressure ratio at the low mass flow.

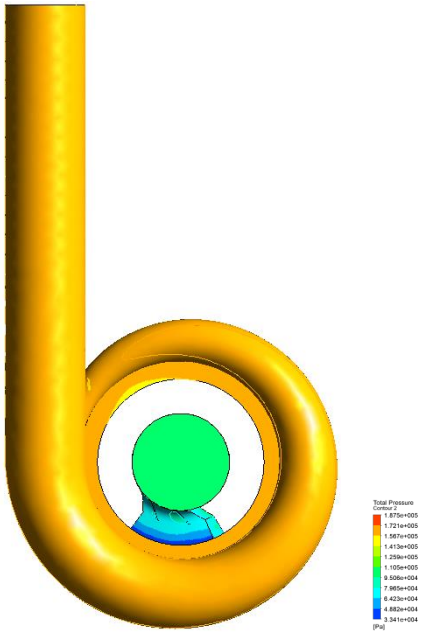

Fig. 23 Non-RCT Compressor Pressure distribution at 140,000rpm and 0.05kg/s

Fig. 24 Non-RCT Compressor Pressure distribution in each cross section of volute at 140,000rpm and 0.05kg/s

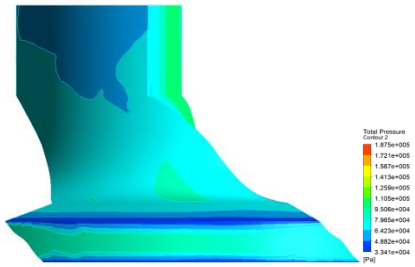

Fig. 25 Non-RCT Impeller Pressure distribution at 140,000rpm and 0.05kg/s

3.6.1.2 Pressure distribution at mass flow rate equal to 0.075kg/s

When the mass flow rate increased to the 0.075kg/s, the compressor volute pressure also increased. In Figure 26, the high pressure area of the compressor volute area is larger than the last section compressor when the mass flow rate equal to the 0.05kg/s. In the volute, the air flow pressure also became higher. The pressure difference between the volute surface and

inside was smaller as shown in Figure 27. At the impeller part, it also shows the small pressure distribution which is shown in Figure 28.

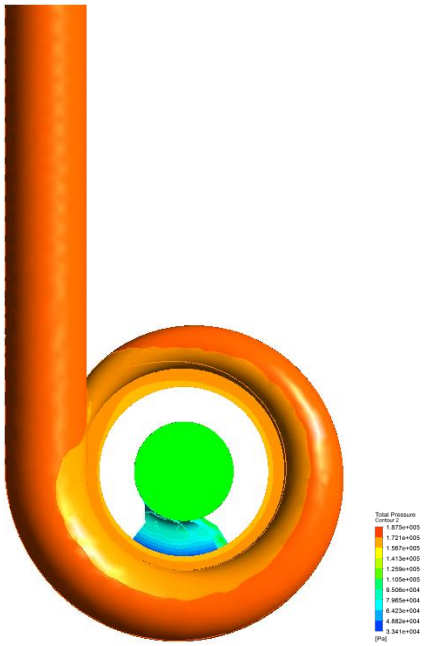

Fig. 26 Non-RCT Compressor Pressure distribution at 140,000rpm and 0.75kg/s

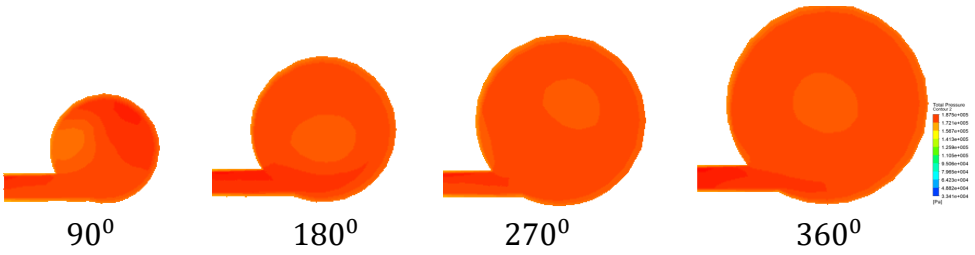

Fig. 27 Non-RCT Compressor Pressure distribution in each cross section of volute at 140,000rpm and 0.075kg/s

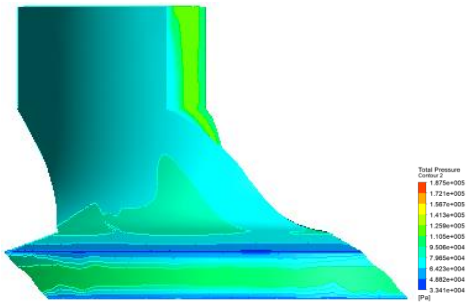

Fig. 28 Non-RCT Impeller Pressure distribution at 140,000rpm and 0.075kg/s

3.6.1.3 Pressure distribution at mass flow rate equal to 0.10kg/s

Figure 29 shows the pressure distribution at 0.10kg/s mass flow rate point. The whole volute part has the high pressure area than compressor at the 0.05kg/s mass flow rate. But still has some smaller part the higher pressure cannot transfer to the volute part. At the volute cross-section part, in the middle area, the volute still has some area pressure is lower than the surface area. And the impeller pressure distribution is shown in Figure 31. In the impeller fluid area, still has smaller pressure at some part. These pressure not uniform parts may cause some loss in the compressor. Even though this 0.10kg/s mass flow rate is the engine maximum power output point.

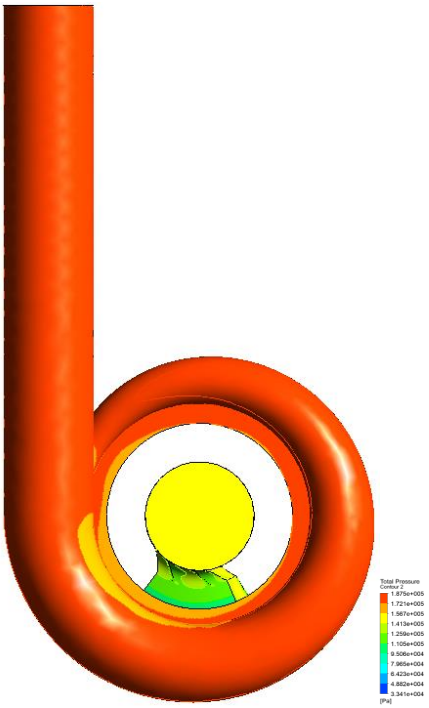

Fig. 29 Non-RCT Compressor Pressure distribution at 140,000rpm and 0.10kg/s

90^0 180^0 270^0 360^0

Fig. 30 Non-RCT Compressor Pressure distribution in each cross-section of volute at 140,000rpm and 0.10kg/s

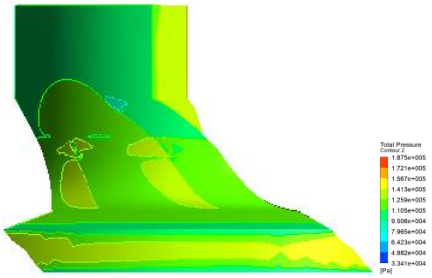

Fig. 31 Non-RCT Impeller Pressure distribution at 140,000rpm and 0.10kg/s

3.6.1.4 Pressure distribution at mass flow rate equal to 0.11kg/s

The highest efficiency mass flow point is 0.11kg/s. In the point, the high pressure can nearly distribute in all vane-ness diffuser and volute part which are shown in Figure 32. In Figure 33, it only has a small pressure difference in the middle line of volute at the volute tongue section. And at the impeller part, the pressure transfer more uniform than 0.05kg/s and 0.075kg/s working mass flow rate.

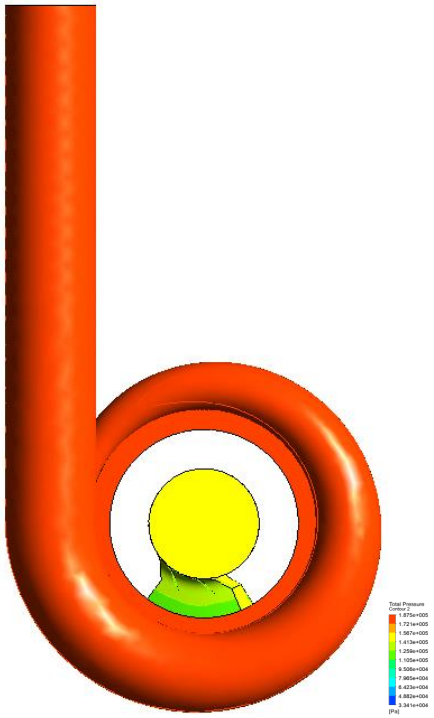

Fig. 32 Non-RCT Compressor Pressure distribution at 140,000rpm and 0.11kg/s

Fig. 33 Non-RCT Compressor Pressure distribution in each cross-section of volute at 140,000rpm and 0.11kg/s

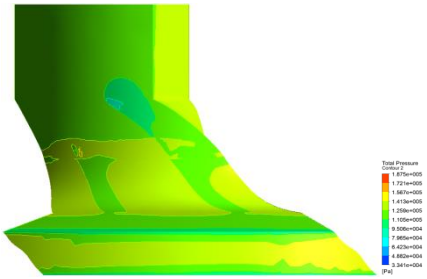

Fig. 34 Non-RCT Impeller Pressure distribution at 140,000rpm and 0.11kg/s

3.6.2 Velocity Vector

The velocity vector would be used to explain the last section the pressure distribution phenomenon.

3.6.2.1 Velocity vector at mass flow rate equal to 0.05kg/s

In Figure 35, it shows the velocity vector at the one passage impeller part and working condition is mass flow rate equal to 0.05kg/s. At the lower mass flow rate, some vortexes occurred in the impeller part, and these vortexes made the compressor unstable and vibration. Figure 36 shows the velocity vector and the compressor inlet duct and Figure 37 shows this part velocity streamline. These two figures indicate that there are some large rotating vortices at the inlet part of the impeller. These large rotating vortices would influence the flow coming into the impeller smoothly. For increasing the compressor low mass flow rate efficiency, these large rotating

vortices should be eliminated or reduced. Inside the compressor volute, the velocity vector of each volute cross-section is shown in Figure 38. At the 90 degrees cross-section, there are two vortexes can be found by the velocity vector in the figure. When the flow comes to the downstream of the volute, the two vortexes become to one. But it still does not have enough energy to let the flow can move to volute surface strongly. This can explain Figure 23 in the last section. The volute surface does not have high pressure.

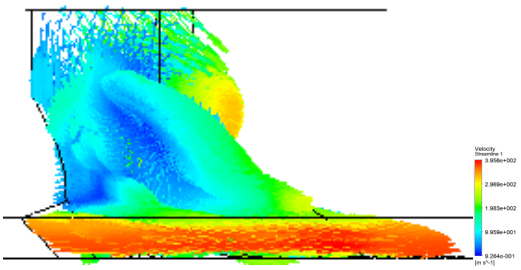

Fig. 35 Non-RCT Impeller velocity vector at 140,000rpm and 0.05kg/s

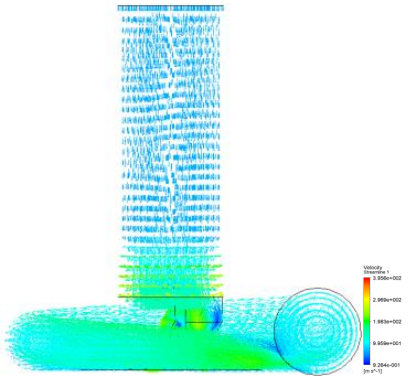

Fig. 36 Non-RCT Inlet duct velocity vector at 140,000rpm and 0.05kg/s

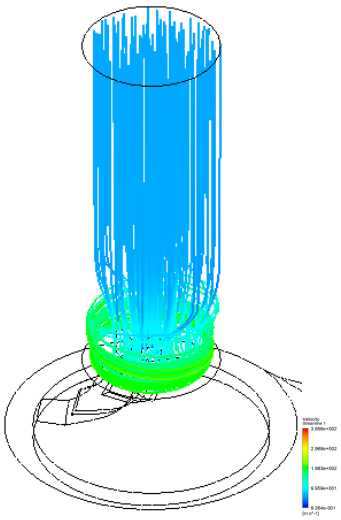

Fig. 37 Non-RCT Inlet duct streamline at 140,000rpm and 0.05kg/s

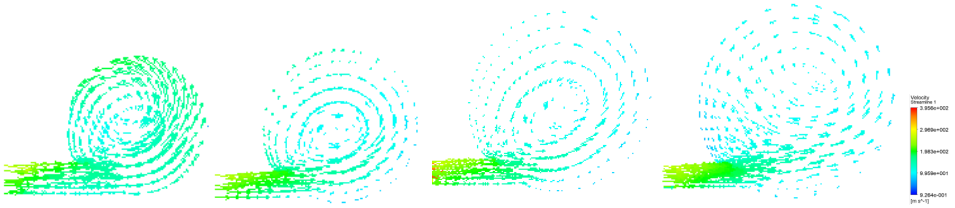

90^0 180^0 270^0 360^0

Fig. 38 Non-RCT Velocity vector in each cross-section of volute at 140,000rpm and 0.05kg/s

3.6.2.3 Velocity vector at mass flow rate equal to 0.075kg/s

When the mass flow rate increased to the 0.075kg/s, the small velocity vortex was still inside the impeller area, which is shown in Figure 39. But the inlet duct swirl flow disappeared at this mass flow rate as shown in

Figure 40 and Figure 41. The velocity vector inside the volute also is similar to mass flow rate equal to 0.05kg/s condition. There is two small vortexes at the 90 degree volute cross section which is shown in Figure 42.

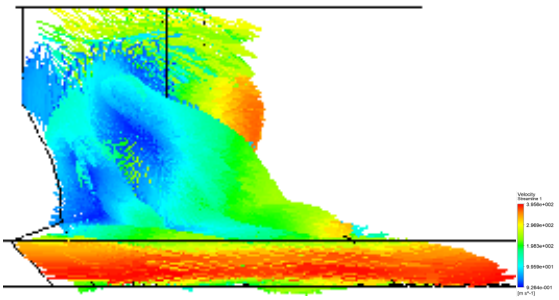

Fig. 39 Non-RCT Impeller velocity vector at 140,000rpm and 0.075kg/s

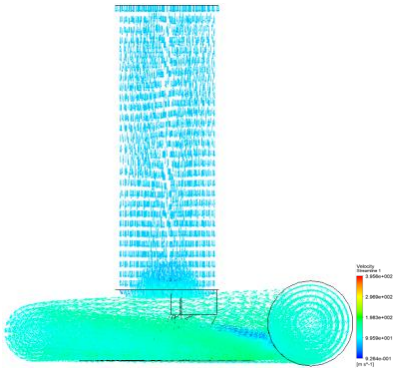

Fig. 40 Non-RCT Inlet duct velocity vector at 140,000rpm and 0.075kg/s

Fig. 41 Non-RCT Inlet duct velocity streamline at 140,000rpm and 0.075kg/s

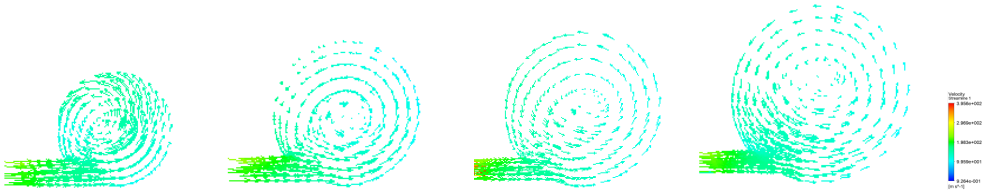

Fig. 42 Non-RCT Non-RCT Velocity vector in each cross section of volute at 140,000rpm and 0.075kg/s

3.6.2.3 Velocity vector at mass flow rate equal to 0.10kg/s

When the mass flow rate increase to the 0.10kg/s, as shown in Figure 43, the lowest velocity vortex area becomes smaller. And highest velocity area is at

the impeller main blade upstream part. In Figure 44, there are no larger vortices at the inlet duct. And in Figure 45 shows the streamline of the inlet duct is straight. This is can explain that the inlet duct straight flow makes the impeller main blade part has the highest velocity area. At this point, there are vibration and larger noise of the compressor. Comparing Figure 46 and Figure 43, at the low mass flow rate the 90^0 volute cross-section two swirl vortexes become to one swirl vortex when the mass flow rate increase to 0.10kg/s. And at the 360^0 *the* volute cross-section, the swirl vortex midpoint is near the volute cross-section midpoint. The volute loss at this mass flow rate is smaller than the last section low mass flow rate.

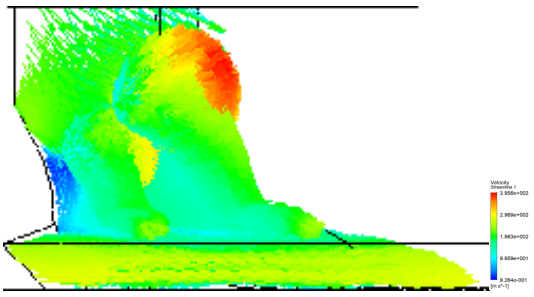

Fig. 43 Non-RCT Impeller velocity vector at 140,000rpm and 0.10kg/s

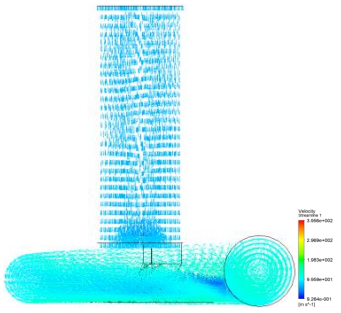

Fig. 44 Non-RCT Inlet duct velocity vector at 140,000rpm and 0.10kg/s

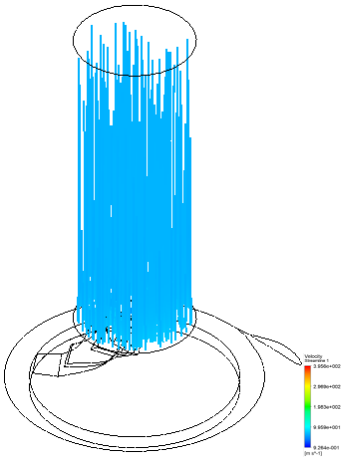

Fig. 45 Non-RCT Inlet duct streamline at 140,000rpm and 0.10kg/s

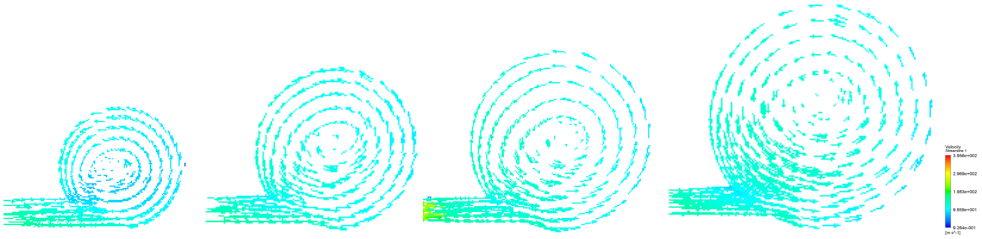

Fig. 46 Non-RCT Velocity vector in each cross-section of volute at 140,000rpm and 0.10kg/s

3.6.2.4 Velocity vector at mass flow rate equal to 0.11kg/s

Figure 47 shows the impeller vector at the 0.11kg/s for the non-RCT compressor. As the mass flow rate increases the vortexes inside the between the impeller blades is decreasing. Only some small parts have very high velocities which are made by the blade tip at the high mass flow rate. The

velocity uniformity is higher than the mass flow rate equal to 0.10kg/s. This can explain from the Figure 48 and Figure 49. At the inlet port, the flow comes to the impeller perpendicularly, so at the impeller blade tip, part would have high-speed area for the interaction between the blade and straight the tip. The velocity vector in each volute cross-section shows that the flow comes to the volute smoothly. And different between the highest and lowest velocity magnitude which is shown at Figure 50 is small than last section working condition. This is also the reason that the highest efficiency of this non-RCT compressor is at this mass flow rate.

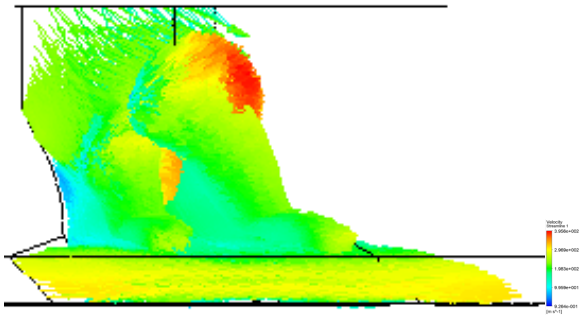

Fig. 47 Non-RCT Impeller velocity vector at 140,000rpm and 0.11kg/s

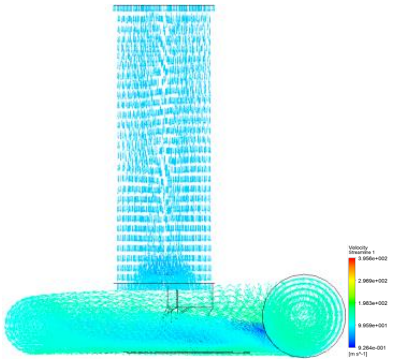

Fig. 48 Non-RCT Inlet duct velocity vector at 140,000rpm and 0.11kg/s

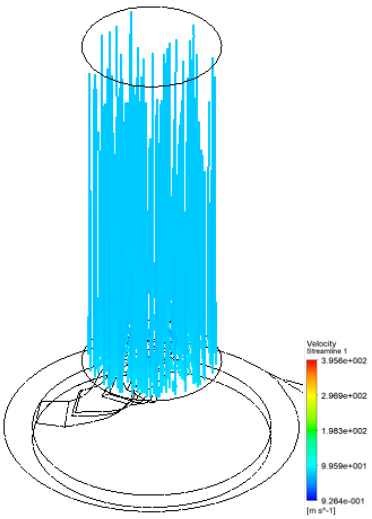

Fig. 49 Non-RCT Inlet duct streamline at 140,000rpm and 0.11kg/s

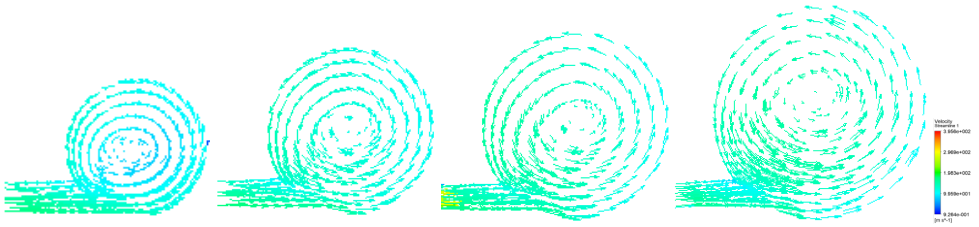

90^0 180^0 270^0 360^0

Fig. 50 Non-RCT Velocity vector in each cross-section of volute at 140,000rpm and 0.11kg/s

3.6.3 Compressor map (Pressure Ratio, Efficiency, Surge margin)

For knowing the whole performance of this Non-RCT compressor, the full range of compressor pressure and efficiency were simulated to get the results. There are 7 compressor RPM option: 60,000 , 80,000 , 100,000 ,

120,000 , 140,000 , 160,000 and 180,000. And the surge line and chock line points are defined each point efficiency equal to 60%. The mass flow range is from 0.01kg/ to 0.17kg/s. The full pressure ratio range map of this Non-RCT compressor is shown in Figure 51. And Figure 52 indicates the full efficiency range map. The pressure ratio and efficiency equation are shown in follow:

$$\text{Pressure Ratio} = \frac{P_{02}}{P_{01}} \tag{13}$$

Efficiency

$$\epsilon = \frac{\left(\frac{P_{02}}{P_{01}}\right)^{\frac{\gamma-1}{\gamma}} - 1}{\frac{T_{02}}{T_{01}} - 1} \tag{14}$$

Where P_{01}=Compressor inlet total pressur

P_{02}= Compressor outlet total pressure

T_{01}= Compressor inlet total temperature

T_{02}= Compressor outlet total temperature

$\gamma =$ Specific heat ratio

The surge margin range equal to:

$$\text{Surge Margin} = \frac{m_{SH} - m_{SL}}{m_{SH}} \tag{15}$$

m_{SH}= mass flow rate at the compressor highest RPM surge point

m_{SL} = mass flow rate at the compressor lowest RPM surge point

The Table 5 and Table 6 show the Non-RCT compressor each operation point pressure ratio and efficiency. The surge margin in this compressor is 0.78.

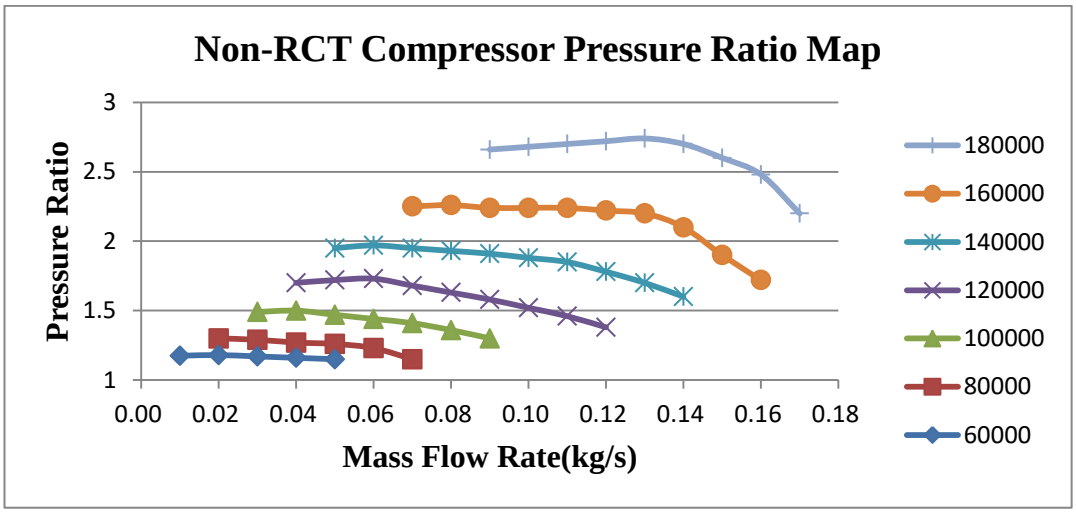

Fig. 51 Non-RCT Compressor Pressure Ratio Map

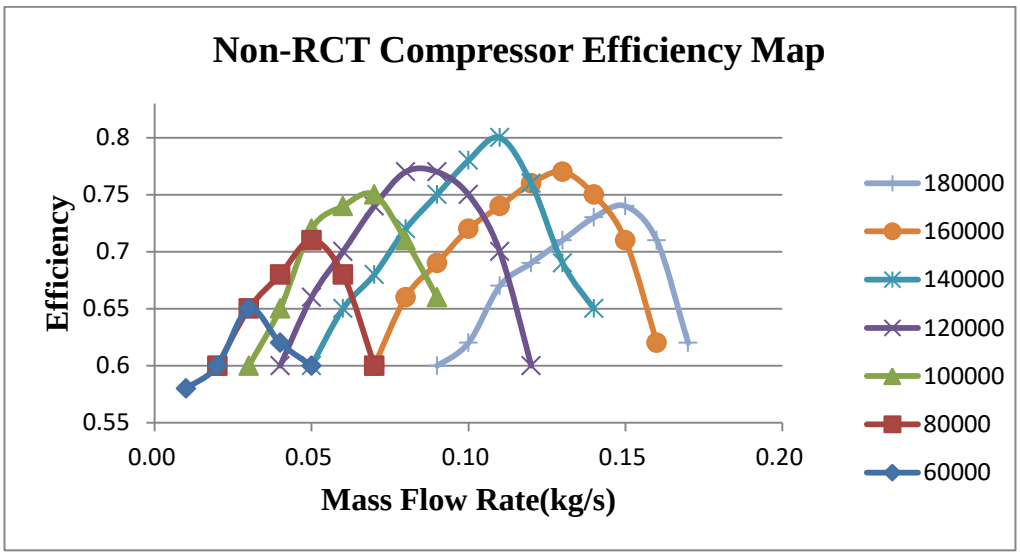

Fig. 52 Non-RCT Compressor Efficiency Map

Table. 5 Non-RCT Compressor Pressure Ratio data

Mass Flow Rate	60,000	80,000	100,000	120,000	140,000	160,000	180,000
0.01	1.18						
0.015	1.18						
0.02	1.18	1.30					
0.03	1.17	1.29	1.49				
0.04	1.16	1.27	1.50	1.70			
0.05	1.15	1.26	1.47	1.72	1.95		
0.06		1.23	1.44	1.73	1.97		
0.07		1.15	1.41	1.68	1.95	2.25	
0.08			1.36	1.63	1.93	2.26	
0.09			1.30	1.58	1.91	2.24	2.66
0.10				1.52	1.88	2.24	2.68
0.11				1.46	1.85	2.24	2.70
0.12				1.38	1.78	2.22	2.72
0.13					1.70	2.20	2.74
0.14					1.60	2.10	2.70

0.15						1.90	2.60
0.16						1.72	2.48
0.17							2.20

Table. 6 Non-RCT Compressor efficiency data

Mass Flow Rate	60,000	80,000	100,000	120,000	140,000	160,000	180,000
0.01	0.58						
0.02	0.59						
0.02	0.6	0.6					
0.03	0.65	0.65	0.6				
0.04	0.62	0.68	0.65	0.6			
0.05	0.6	0.71	0.72	0.66	0.6		
0.06		0.68	0.74	0.7	0.65		
0.07		0.6	0.75	0.74	0.68	0.6	
0.08			0.71	0.77	0.72	0.66	
0.09			0.66	0.77	0.75	0.69	0.6
0.1				0.75	0.78	0.72	0.62
0.11				0.7	0.8	0.74	0.67
0.12				0.6	0.76	0.76	0.69

0.13					0.69	0.77	0.71
0.14					0.65	0.75	0.73
0.15						0.71	0.74
0.16						0.62	0.71
0.17							0.62

3.7 Summary

In this section, the Basic model Non-RCT compressor was simulated. The results show that the Non-RCT compressor has the vortex between the impeller blades at the low mass flow rate. And the full range of compressor map was made to know this compressor performance.

Chapter 4 Simulation of RCT turbocharger compressor

From the chapter 3, the basic non-RCT turbocharger has some disadvantage. So, the Recirculation Casing Treatment compressor is designed in this chapter to reduce the stable flow at the low mass flow rate operating condition.

4.1 RCT compressor geometry and mesh

Figure 53 shows the RCT geometry. There is channel connecting the impeller blade area and compressor inlet duct. The fluid domain of the RCT compressor is shown in Figure 54. The mesh was generated by the same method with Non-RCT compressor. RCT total mesh grids are 1,139,993. The one impeller passage has 696,647 mesh grids. Volute mesh number is 178,547. RCT and inlet duct have 264,799 mesh grids. Figure 55 shows the mesh of this RCT compressor and detail view of the RCT part.

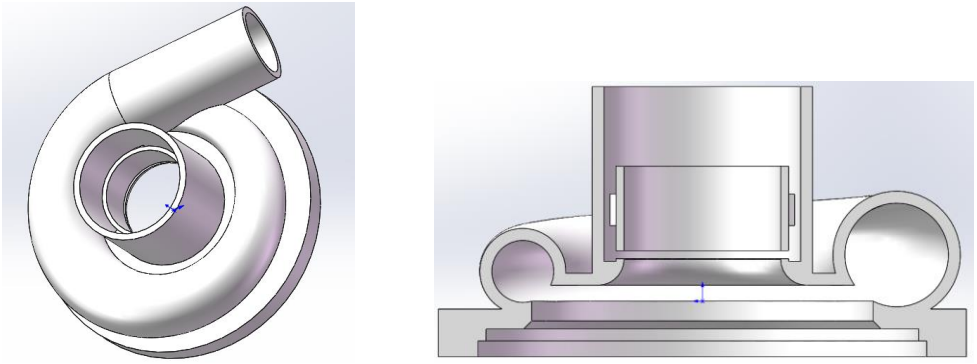

Fig. 53 RCT Compressor geometry

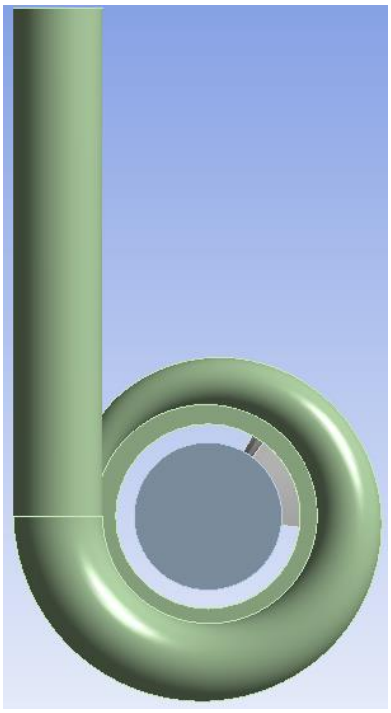

Fig. 54 RCT Compressor fluid domain

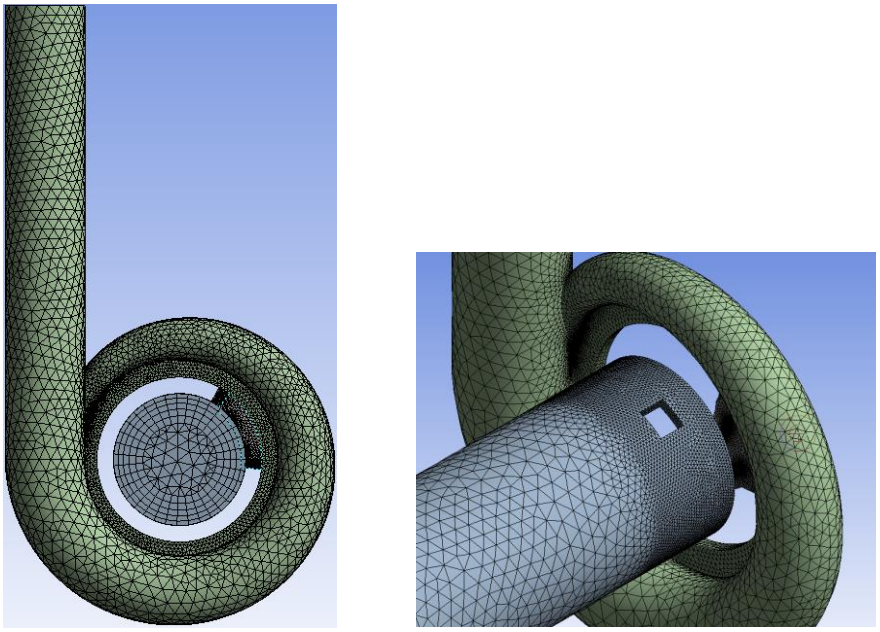

Fig. 55 RCT Compressor mesh

4.2 Simulation Results and Comparison

4.2.1 Pressure distribution

4.2.1.1 Pressure distribution at mass flow rate equal to 0.05kg/s

Figure 56 shows the RCT compressor pressure distribution. The surface of the volute pressure is higher than the Non-RCT compressor. From Figure 57, the pressure magnitude difference is smaller than the Non-RCT compressor. At the impeller pressure distribution, the RCT compressor impeller pressure is higher than the Non-RCT one as shown in Figure 58. The phenomenon indicates the RCT compressor has better performance at the low mass flow rate.

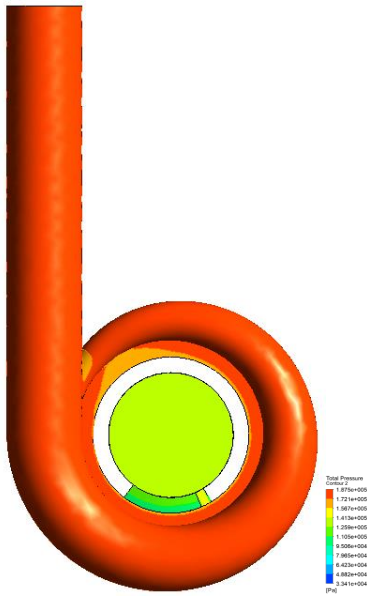

Fig. 56 RCT Compressor Pressure distribution at 140,000rpm and 0.05kg/s

Fig. 57 RCT Compressor Pressure distribution in each cross section of volute at 140,000rpm and 0.05kg/s

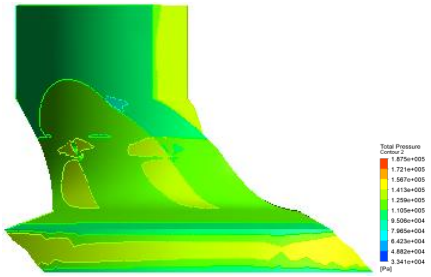

Fig. 58 RCT Impeller Pressure distribution at 140,000rpm and 0.05kg/s

4.2.1.2 Pressure distribution at mass flow rate equal to 0.075kg/s

The compressor pressure at the mass flow rate 0.075kg/s of the RCT compressor is also higher and uniform than the Non-RCT compressor which is shown in Figure 59. As the mass flow increased, the volute inside pressure also increased as shown in Figure 60. The impeller pressure distribution indicates the higher pressure magnitude than the Non-RCT compressor which is shown in Figure 61.

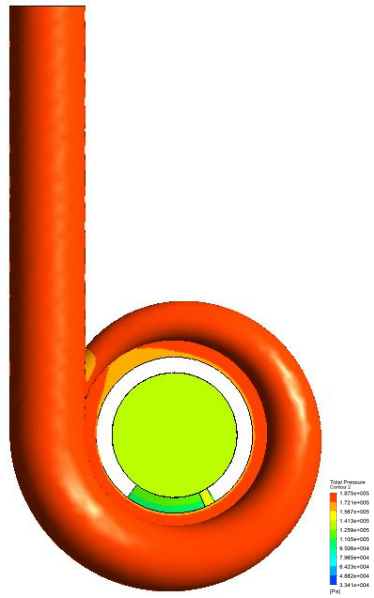

Fig. 59 RCT Compressor Pressure distribution at 140,000rpm and 0.075kg/s

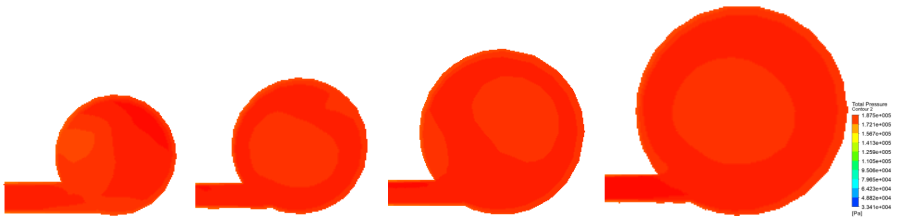

Fig. 60 RCT Compressor Pressure distribution in each cross-section of volute at 140,000rpm and 0.075kg/s

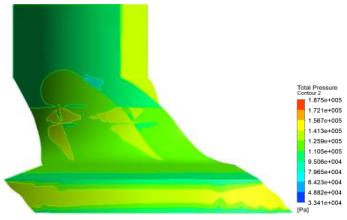

Fig. 61 RCT Impeller Pressure distribution at 140,000rpm and 0.075kg/s

4.2.1.3 Pressure distribution at mass flow rate equal to 0.10kg/s

In this part, at the medium mass flow rate point, the RCT compressor still has the good performance of the pressure distribution. From Figure 62 to Figure 64 show that all volute part has high pressure. Inside the volute, the pressure magnitude increases uniformly. But at the impeller part, there are some small areas have the not very uniform pressure distribution.

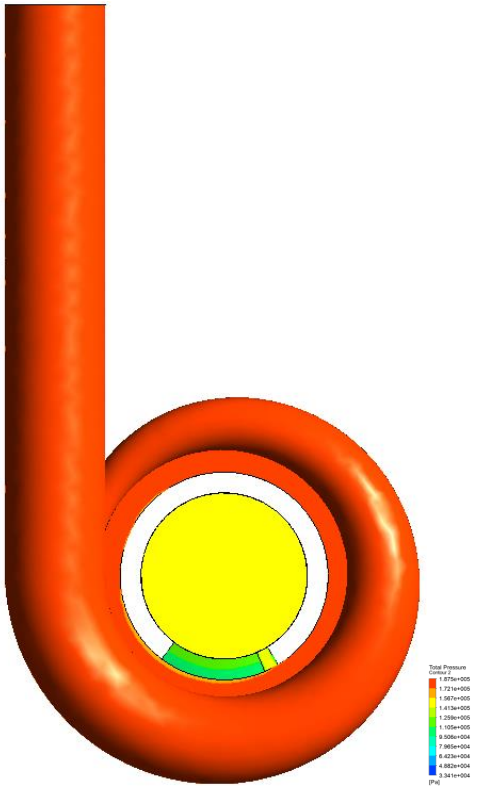

Fig. 62 RCT Compressor Pressure distribution at 140,000rpm and 0.10kg/s

90^0 180^0 270^0 360^0

Fig. 63 RCT Compressor Pressure distribution in each cross-section of volute at 140,000rpm and 0.10kg/s

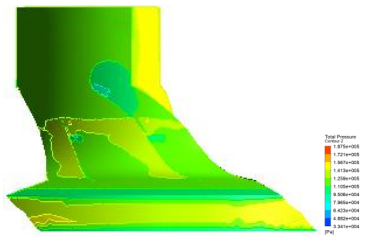

Fig. 64 RCT Impeller Pressure distribution at 140,000rpm and 0.10kg/s

4.2.1.4 Pressure distribution at mass flow rate equal to 0.11kg/s

In Figure 65, there are some lower pressure areas where near the downstream of the volute part. Inside the magnitude difference is higher than the 0.10kg/s working condition, especially at the downstream volute cross-section which is shown in Figure 66. There are also some small areas have the not very uniform pressure distribution in impeller part as shown in Figure 67.

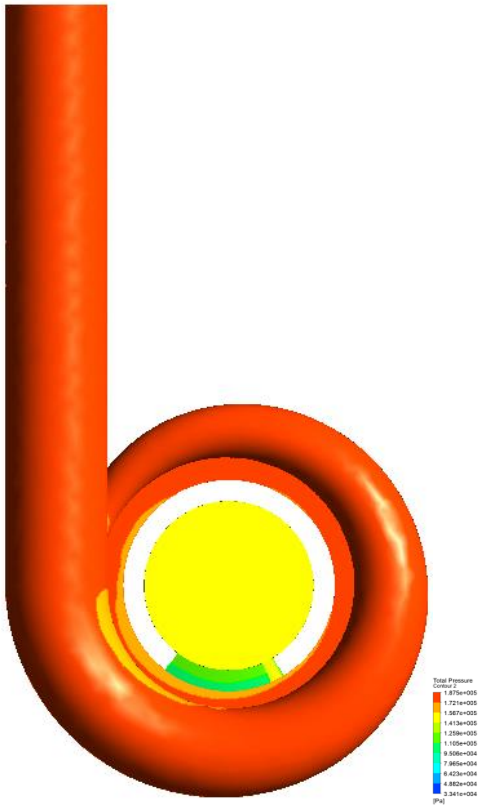

Fig. 65 RCT Compressor Pressure distribution at 140,000rpm and 0.11kg/s

Fig. 66 RCT Compressor Pressure distribution in each cross-section of volute at 140,000rpm and 0.11kg/s

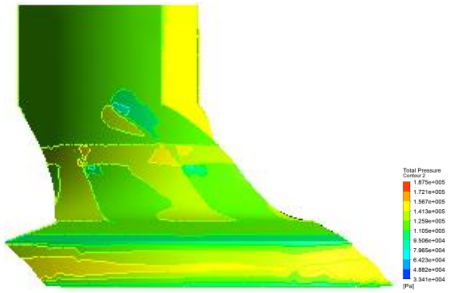

Fig. 67 RCT Impeller Pressure distribution at 140,000rpm and 0.11kg/s

4.2.2 Velocity Vector

4.2.2.1 Velocity vector at mass flow rate equal to 0.05kg/s

The Non-RCT compressor at a low mass flow rate, there are a lot of small vortexes in the impeller part. By adopting the RCT, in Figure 68 shows the area of vortexes become smaller. The vortexes flow comes through the RCT channel and returns to the inlet duct again. The detail of the flow movement inside the RCT is shown in Figure 71. As shown in Figure 69 and Figure 70, in the compressor inlet duct, the larger vortices at the inlet impeller inlet area disappear. And air becomes a larger swirl into the impeller. This can decrease the vibration and noisy of the impeller at a low mass flow rate. The volute cross-section velocity vectors are shown in Figure 72. The second vortex in the 90° the cross-section is not very obvious.

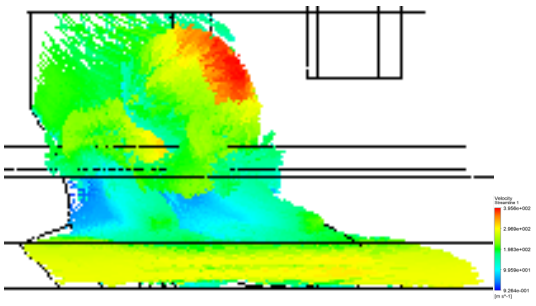

Fig. 68 RCT Impeller velocity vector at 140,000rpm and 0.05kg/s

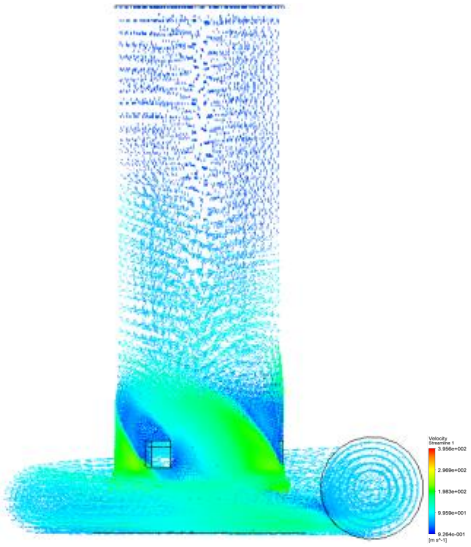

0.05 kg/s

Fig. 69 RCT Inlet duct velocity vector at 140,000rpm and 0.05kg/s

Fig. 70 RCT Inlet duct streamline at 140,000rpm and 0.05kg/s

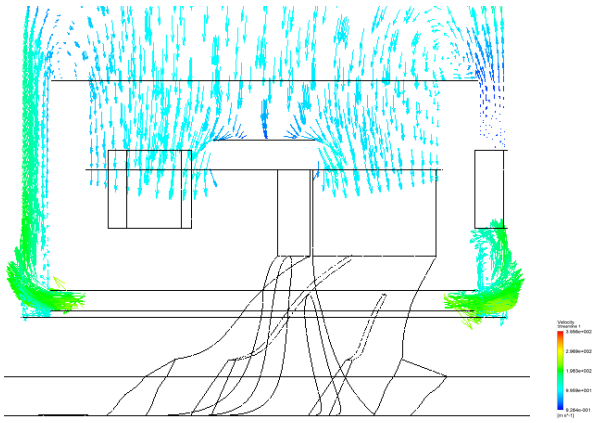

Fig.71 RCT velocity vector at 140,000rpm and 0.05kg/s

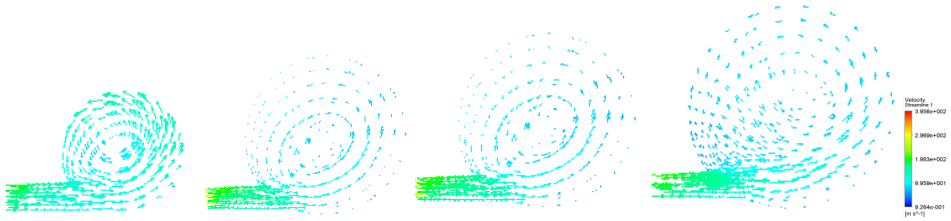

90^0 180^0 270^0 360^0

Fig. 72 RCT Velocity vector in each cross-section of volute at 140,000rpm and 0.05kg/s

4.2.2.2 Velocity vector at mass flow rate equal to 0.075kg/s

Comparing the Non-RCT compressor at the 0.075kg/s mass flow rate point, the RCT compressor also avoids many small velocity vortexes inside the impeller part as shown in Figure 73. The swirling flow at the inlet duct diminished as shown in Figure 74 and Figure 75. In Figure 76, there is still a lot of coming through the RCT slot from the impeller part to the inlet duct. The 90 degree volute cross section vortex increased more than the Non-RCT compressor which is shown in Figure 77.

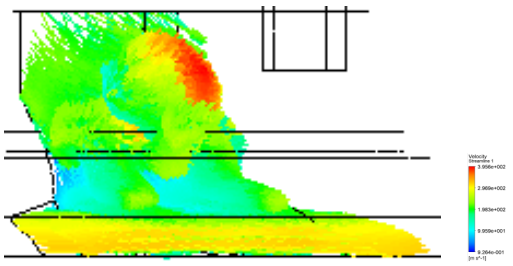

Fig. 73 RCT Impeller velocity vector at 140,000rpm and 0.075kg/s

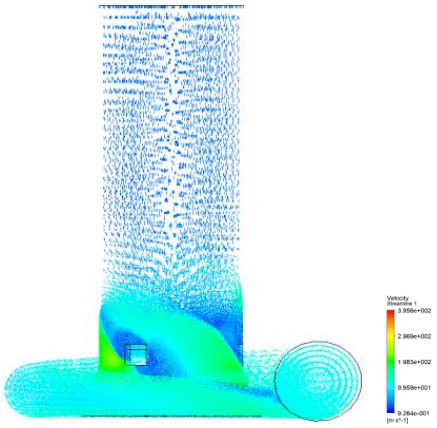

Fig. 74 RCT Inlet duct velocity vector at 140,000rpm and 0.075kg/s

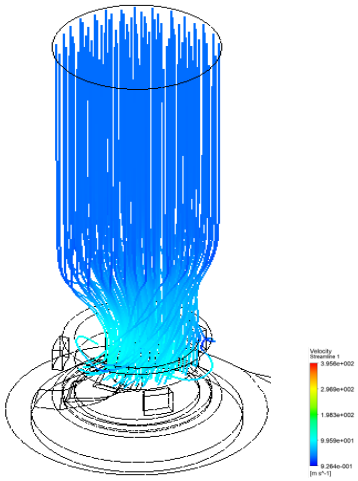

Fig. 75 RCT Inlet duct streamline at 140,000rpm and 0.0750kg/s

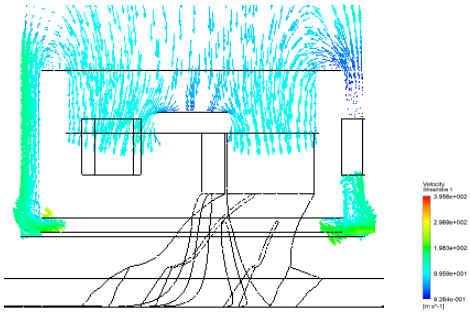

Fig. 76 RCT velocity vector at 140,000rpm and 0.075kg/s

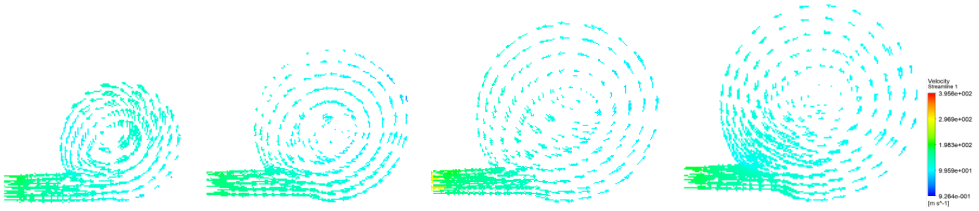

90^0 180^0 270^0 360^0

Fig. 77 RCT Velocity vector in each cross-section of volute at 140,000rpm and 0.075kg/s

4.2.2.3 Velocity vector at mass flow rate equal to 0.10kg/s

At the medium working mass flow rate condition, the RCT also can avoid the low-velocity vortexes as shown in Figure 78. There are three fixed ribs inside the RCT. These ribs would make strong swirl the flow inside the RCT which is shown in Figure 79 and Figure 80. This phenomenon may cause the compressor efficiency decrease at the medium and high mass flow rate. Figure 82 indicates the RCT compressor volute flow distribution is similar to the Non-RCT compressor.

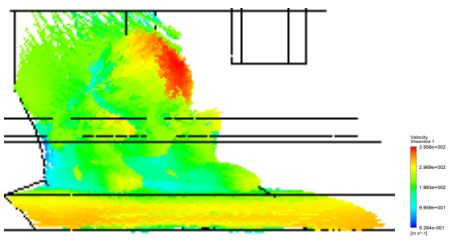

Fig. 78 RCT Impeller velocity vector at 140,000rpm and 0.10kg/s

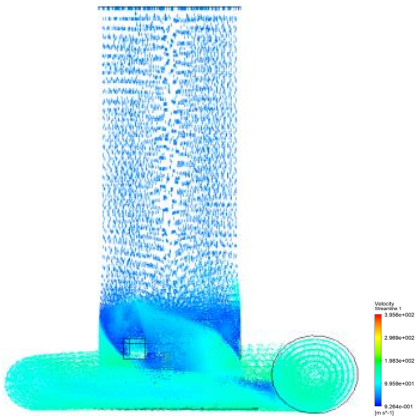

Fig. 79 RCT Inlet duct velocity vector at 140,000rpm and 0.10kg/s

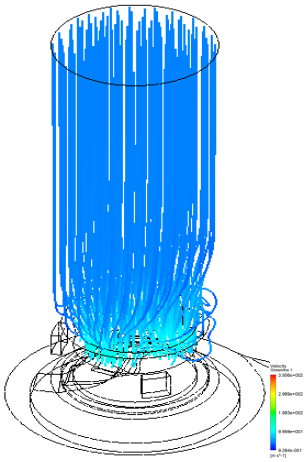

Fig. 80 RCT Inlet duct streamline at 140,000rpm and 0.10kg/s

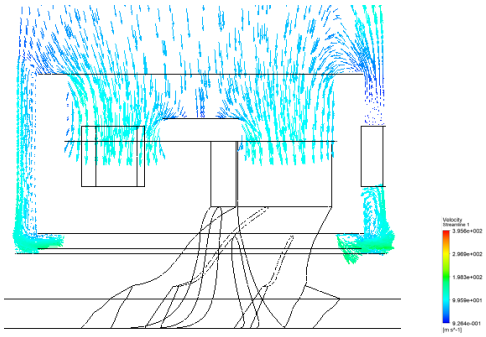

Fig.81 RCT velocity vector at 140,000rpm and 0.10kg/s

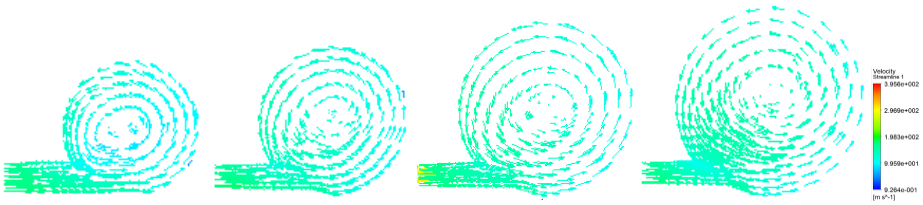

90^0 180^0 270^0 360^0

Fig. 82 RCT Velocity vector in each cross-section of volute at 140,000rpm and 0.10kg/s

4.2.2.4Velocity vector at mass flow rate equal to 0.11kg/s

As the mass flow rate increase, the RCT avoiding the vortexes inside the impeller part ability becomes weaken. In Figure 83 shows there are still have some vortexes inside the impeller in RCT compressor. Figure 84 and Figure 85 show the inlet duct air flow comes to impeller straightly. The inlet duct flow and RCT return flow mix together. And fixed ribs inside the RCT make this mixed flow separately. This uniform flow inside the RCT would decrease the efficiency of compressor. Inside the volute part, there are also not much different from the Non-RCT compressor as shown in Figure 87.

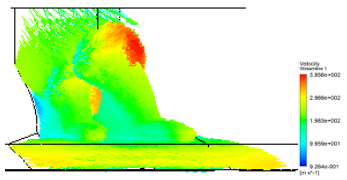

Fig. 83 RCT Impeller velocity vector at 140,000rpm and 0.11kg/s

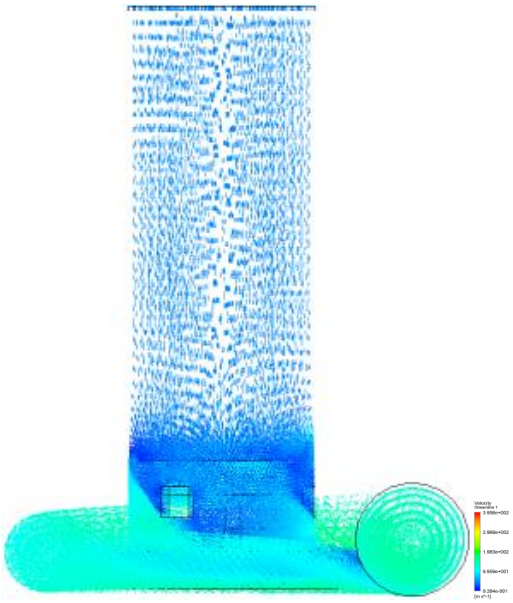

Fig. 84 RCT Inlet duct velocity vector at 140,000rpm and 0.11kg/s

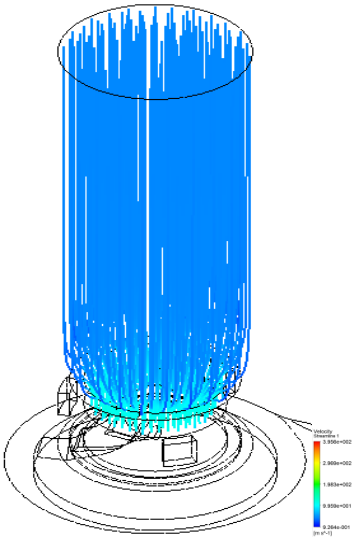

Fig. 85 RCT Inlet duct streamline at 140,000rpm and 0.11kg/s

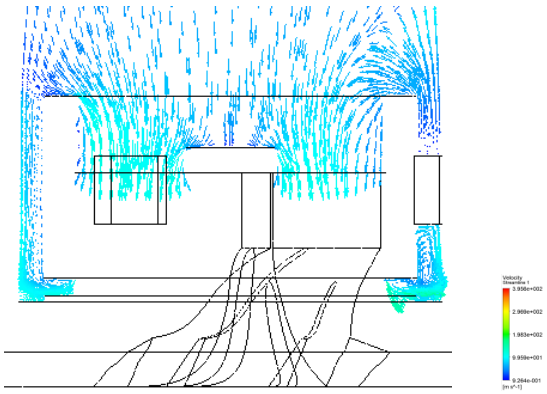

Fig.86 RCT velocity vector at 140,000rpm and 0.11kg/s

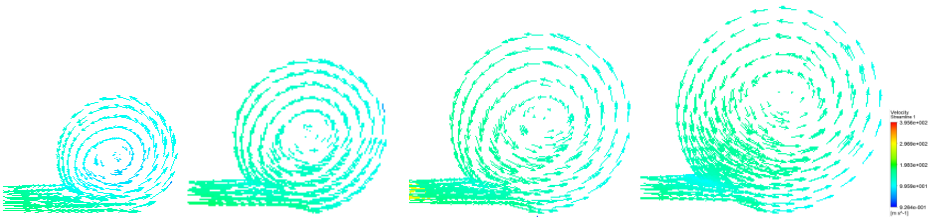

Fig. 87 RCT Velocity vector in each cross-section of volute at 140,000rpm and 0.11kg/s

4.2.3 Optimization design of RCT compressor

The operation point of optimization design is the design point which RPM equal to 140,000 and mass flow rate is 0.10kg/s. The optimization method is the Design of Experiment（DOE） Taguchi orthogonal optimum design. There are three factors: RCT channel width (Rw), RCT slot height (Rh) and RCT slot height from the diffuser (RH) as shown in Figure 88. Table 7 shows the each factor has three level dimensions.

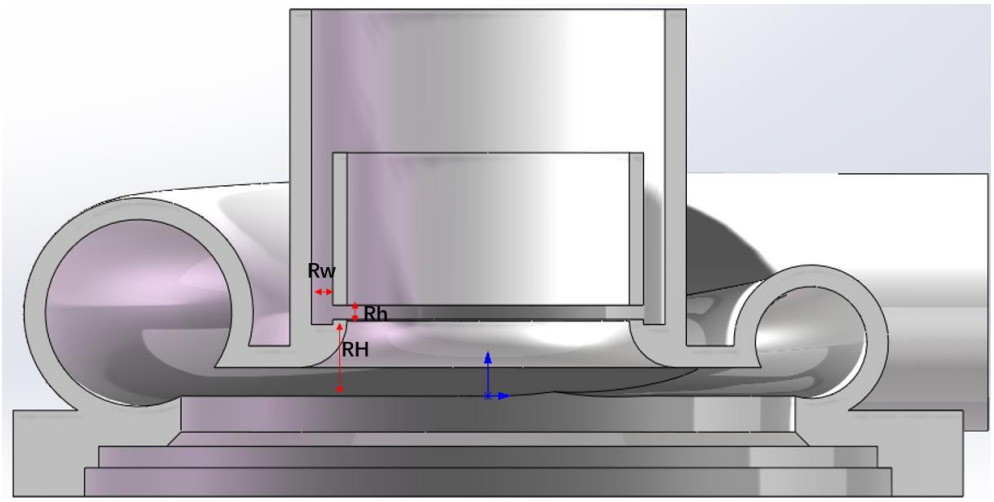

Fig.88 RCT compressor factor for DOE optimization design

Table 7 RCT compressor level data of each factor

Factor	A=Rw(mm)	B=Rh(mm)	C=RH(mm)
Level 1	2	2	10
Level 2	3	3	11
Level 3	4	4	12

Table 8 shows the response for the pressure ratio, the best dimensions is A1 B2.5 and C2.5 which the real size is Rw=2mm, Rh=3.5mm, and RH=11.5mm. Figure 89 shows the main mean of pressure ratio effects plot for RCT compressor. The A factor which is RCT channel width (Rw), is more sensitivity for the RCT compressor pressure ratio. And Table 9 indicates the response for the efficiency means. The optimization choose is A1 B3 C2 which the real size is Rw=2mm, Rh=4mm, and RH=12mm. For

the efficiency, the RCT channel width (Rw), RCT slot height from the diffuser (RH) are more sensitive. At the design point, the RCT compressor is lower than the Non-RCT compressor. The optimization design for the RCT compressor first thinks about the efficiency response. The final optimization of the RCT compressor is Rw=2mm, Rh=4mm, and RH=12mm.

Table 8 RCT Response for Pressure Ratio Means

Level	A	B	C
1	1.877	1.867	1.870
2	1.860	1.870	1.867
3	1.873	1.873	1.873
Delta	0.017	0.007	0.007
Rank	1	2.5	2.5

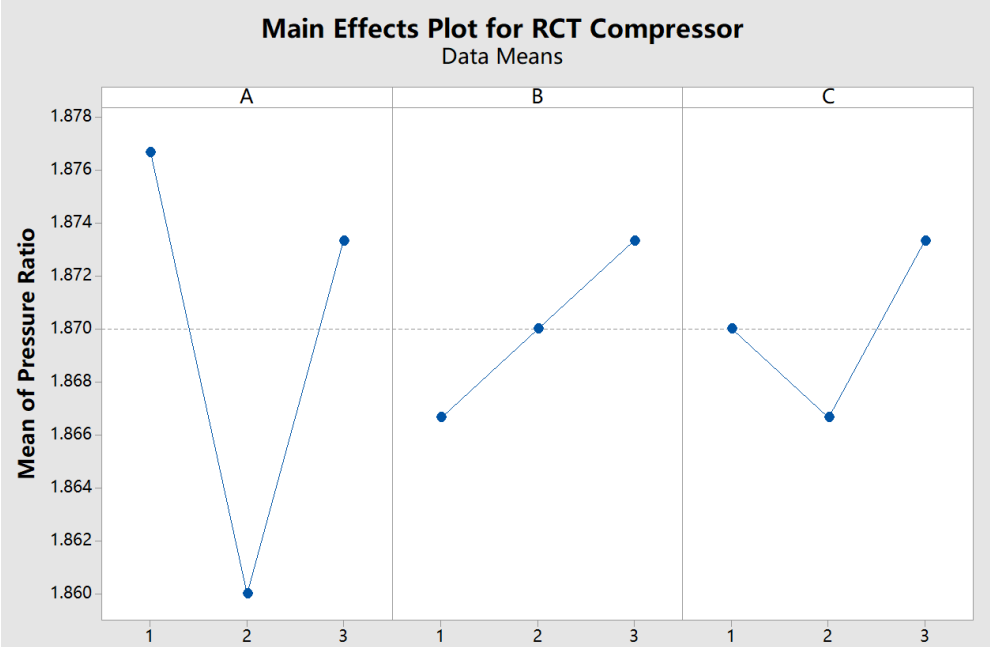

Fig.89 Main mean of pressure ratio effects plot for RCT compressor

Table 9 RCT Response for Efficiency Means

Level	A	B	C
1	0.7300	0.7300	0.7233
2	0.7200	0.7300	0.7267
3	0.7333	0.7233	0.7333
Delta	0.0133	0.0067	0.0100
Rank	1	3	2

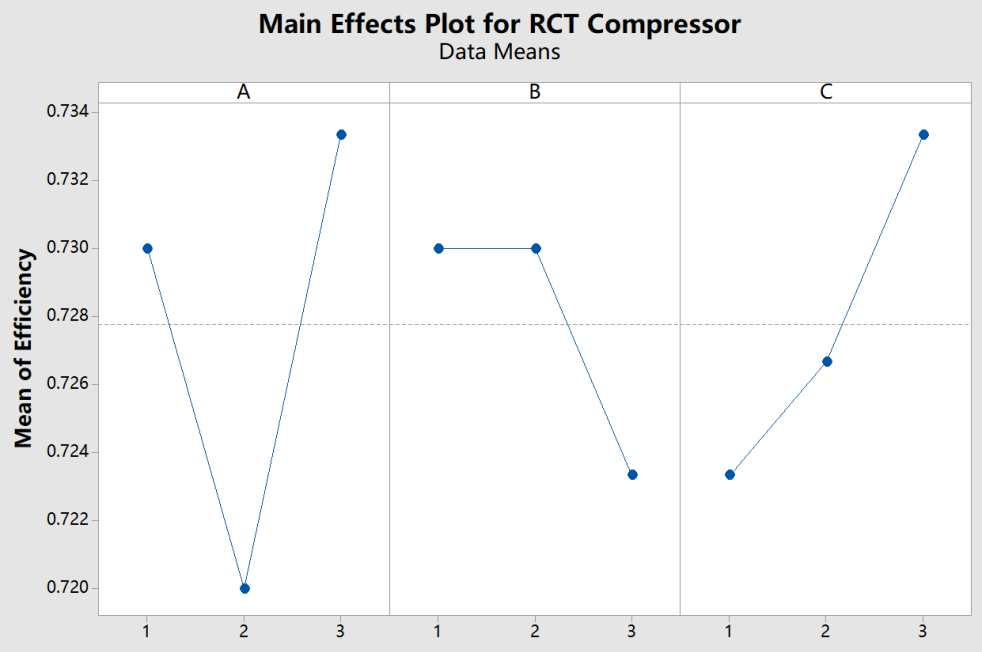

Fig.90 Main mean of efficiency effects plot for RCT compressor

4.2.4 Compressor map (Pressure Ratio, Efficiency, Surge margin)

After using the optimization design the dimensions of RCT compressor. The optimized RCT compressor used to get the full range compressor map. Figure 91 shows the pressure ratio compressor map of the RCT compressor. The surge margin of this RCT compressor is 0.83 which is higher than the Non-RCT compressor. Table 10 shows the exactly pressure ratio data for each simulation point. The compressor efficiency map is shown in Figure 92 and the data is shown in Table 11. For efficiency, the RCT compressor at

the low range mass flow rate which is from 0.01kg/s to 0.06 kg/s is higher than the Non-RCT compressor, but at the middle and high mass flow rate range which is smaller than the Non-RCT one. Especially at the middle mass flow rate, the RCT compressor can be reduced two or three percentage efficiency than the Non-RCT compressor.

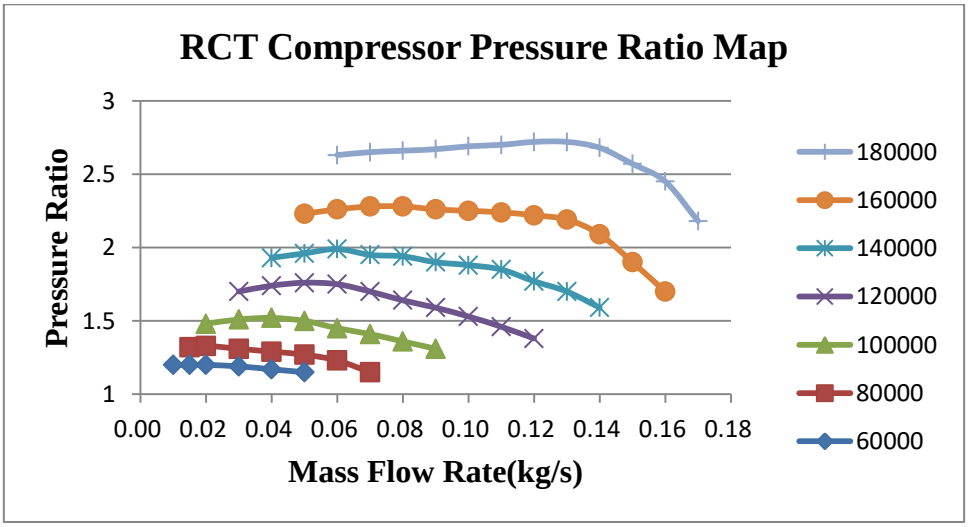

Fig. 91 RCT Compressor Pressure Ratio Map

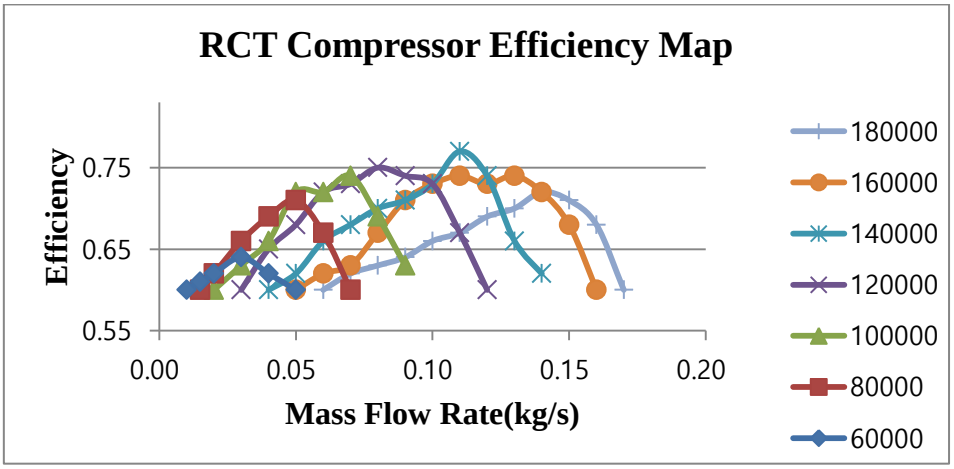

Fig. 92 RCT Compressor Efficiency Map

Table. 10 RCT Compressor Pressure Ratio data

Mass Flow Rate	60,000	80,000	100,000	120,000	140,000	160,000	180,000
0.01	1.20						
0.015	1.20	1.32					
0.02	1.20	1.33	1.48				
0.03	1.19	1.31	1.51	1.70			
0.04	1.17	1.29	1.52	1.74	1.93		
0.05	1.15	1.27	1.50	1.76	1.96	2.23	
0.06		1.23	1.45	1.75	1.99	2.26	2.63
0.07		1.15	1.41	1.70	1.95	2.28	2.65
0.08			1.36	1.64	1.94	2.28	2.66
0.09			1.31	1.59	1.90	2.26	2.67
0.10				1.53	1.88	2.25	2.69
0.11				1.46	1.85	2.24	2.70
0.12				1.38	1.77	2.22	2.72
0.13					1.70	2.19	2.72
0.14					1.59	2.09	2.68
0.15						1.90	2.57
0.16						1.70	2.45
0.17							2.18

Table. 11 RCT Compressor efficiency data

Mass Flow Rate	60,000	80,000	100,000	120,000	140,000	160,000	180,000
0.01	0.6						
0.02	0.61	0.6					
0.02	0.62	0.62	0.6				
0.03	0.64	0.66	0.63	0.6			
0.04	0.62	0.69	0.66	0.65	0.6		
0.05	0.6	0.71	0.72	0.68	0.62	0.6	
0.06		0.67	0.72	0.72	0.66	0.62	0.6
0.07		0.6	0.74	0.73	0.68	0.63	0.62
0.08			0.69	0.75	0.7	0.67	0.63
0.09			0.63	0.74	0.71	0.71	0.64
0.1				0.73	0.73	0.73	0.66
0.11				0.67	0.77	0.74	0.67
0.12				0.6	0.74	0.73	0.69
0.13					0.66	0.74	0.7
0.14					0.62	0.72	0.72
0.15						0.68	0.71
0.16						0.6	0.68
0.17							0.6

4.3 Summary

The RCT compressor can increase the surge margin range and avoid the vortex inside the impeller at low mass flow rate. But it has lower efficiency at the middle flow range mass flow rate for it has the swirl flow and the inlet duct. The optimization design can increase the RCT efficiency at the design point.

Chapter 5 CFD simulation of Hybrid RCT turbocharger compressor

In last chapter, the CFD simulation results indicate the RCT compressor has larger surge margin area than the non-RCT model, but the efficiency of RCT compressor is lower than the non-RCT model at the middle range working mass flow rate. The new design of compressor is shown in this chapter to increase the RCT middle mass flow rate efficiency.

5.1 Hybrid-RCT compressor geometry and mesh

The geometry of Hybrid-RCT is shown in Figure 93. This new design of compressor included two parts. One is RCT and another is a channel connecting the downstream of volute and RCT. Figure 94 shows the fluid domain of Hybrid-RCT compressor. Hybrid RCT compressor total mesh grids are 1,154,920. The one impeller passage has 696,647 mesh grids. Volute, Hybrid RCT and inlet duct total mesh grids are 458,273 which are shown in Figure 95.

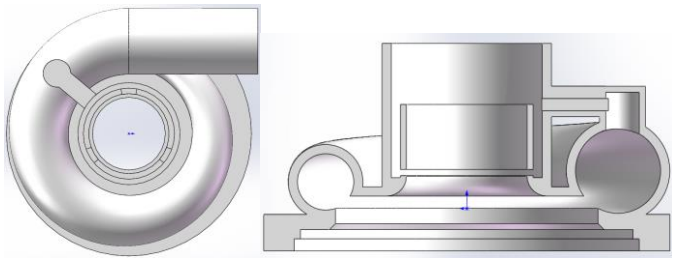

Fig. 93 Hybrid RCT Compressor geometry

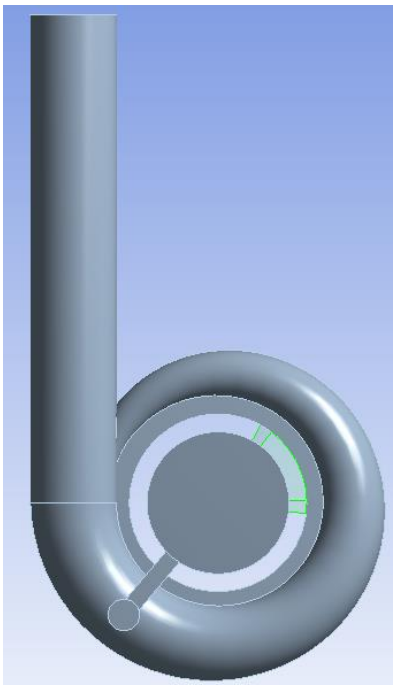

Fig. 94 Hybrid RCT Compressor fluid domain

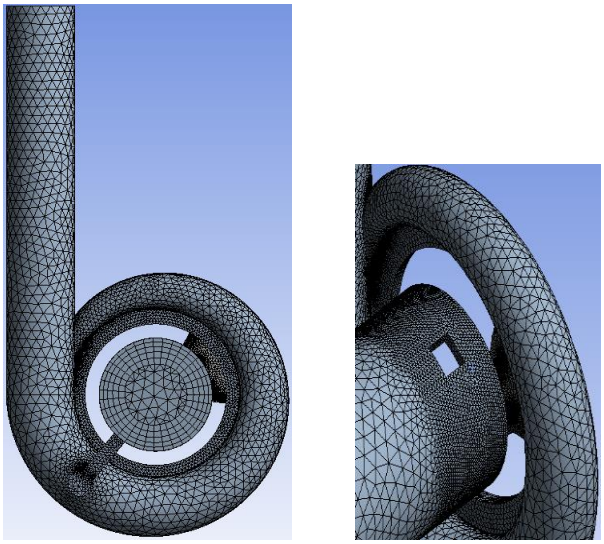

Fig. 95 Hybrid RCT Compressor mesh

5.2 Simulation Results and Comparison

In this section, three type of compressor: Hybrid RCT, RCT and Non-RCT would be compared and discussed.

5.2.1 Pressure distribution

5.2.1.1 Pressure distribution at mass flow rate equal to 0.05kg/s

As shown in Figure 96, at the near the surge point, the RCT and Hybrid RCT have a large area for high pressure, especially the volute surface. Comparing the cross-section of the volute, the Hybrid RCT compressor has a higher pressure inside the volute and more uniform pressure distribution in each cross-section which shown in Figure 97. In the impeller part, the Hybrid RCT and RCT compressor impeller have high pressure magnitude than the Non-RCT one as shown in Figure 98.

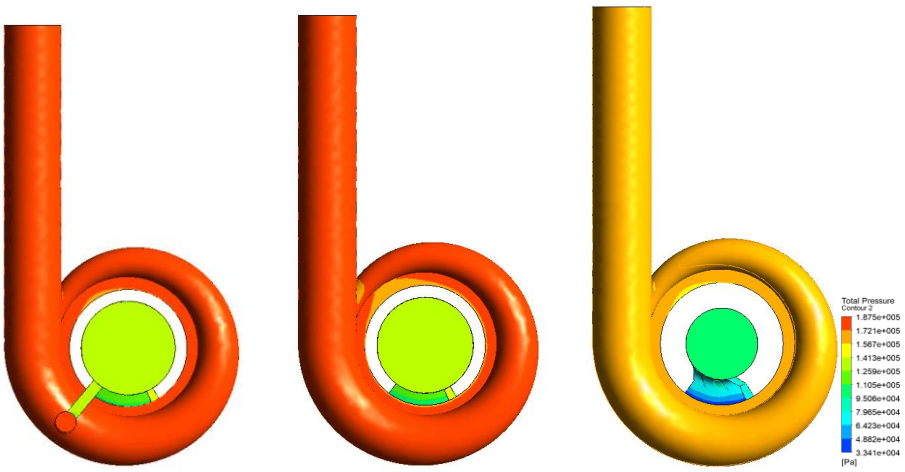

Hybrid RCT RCT Non-RCT

Fig. 96 Compressor Pressure distribution at 140,000rpm and 0.05kg/s

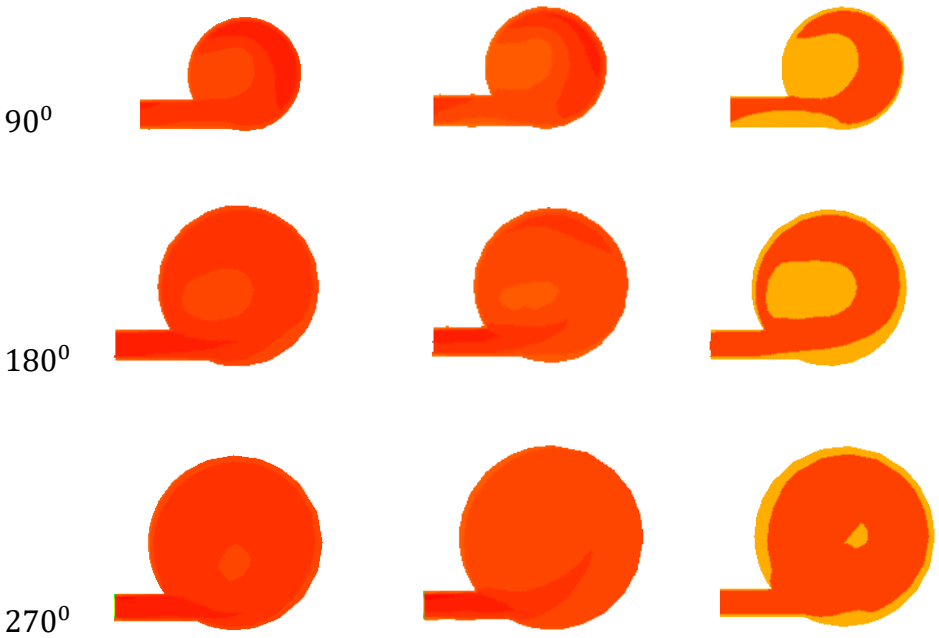

Hybrid RCT RCT Non-RCT

Fig. 97 Compressor Pressure distribution in each cross-section of volute at 140,000rpm and 0.05kg/s

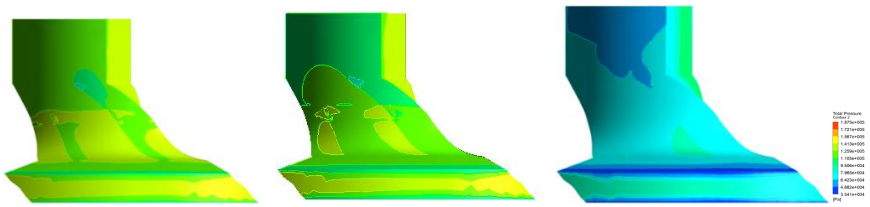

Hybrid RCT RCT Non-RCT

Fig. 98 Impeller Pressure distribution at 140,000rpm and 0.05kg/s

5.2.1.2 Pressure distribution at mass flow rate equal to 0.075kg/s

In this operation mass flow rate, the Hybrid RCT and RCT compressor also showed the higher volute surface pressure distribution as shown in Figure 99. The Hybrid RCT has the most uniform pressure distribution inside the compressor volute part which is shown in Figure 100. In the Figure 101, comparing the impeller pressure distribution, the Hybrid RCT and RCT

have the higher pressure area than the Non-RCT compressor.

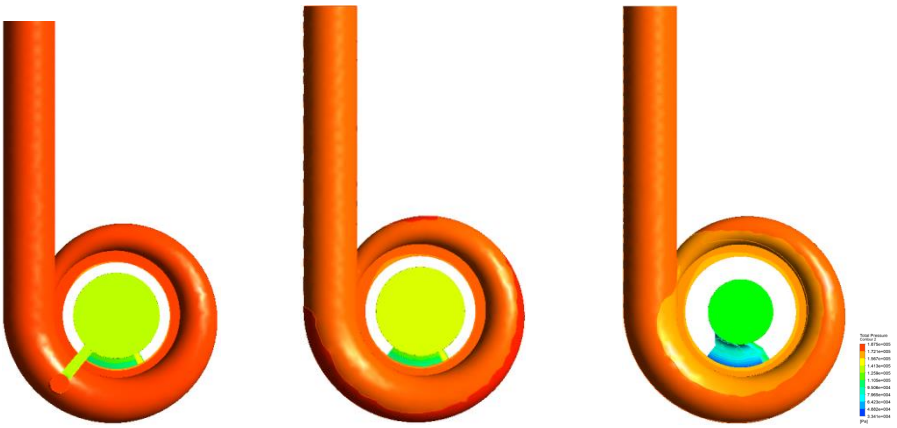

Hybrid RCT RCT Non-RCT

Fig. 99 Compressor Pressure distribution at 140,000rpm and 0.075kg/s

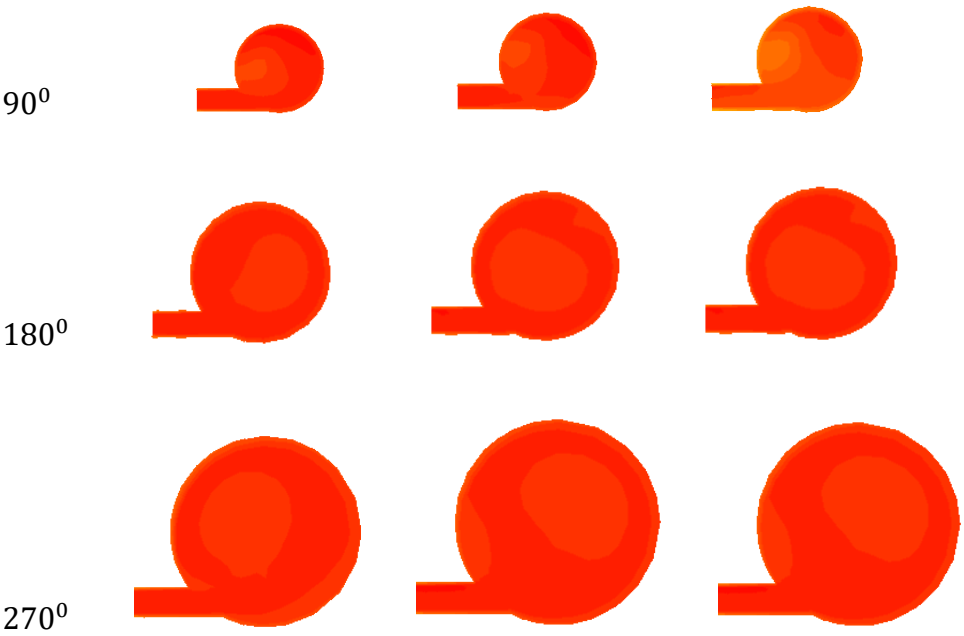

Fig. 100 Compressor Pressure distribution in each cross section of volute at 140,000rpm and 0.075kg/s

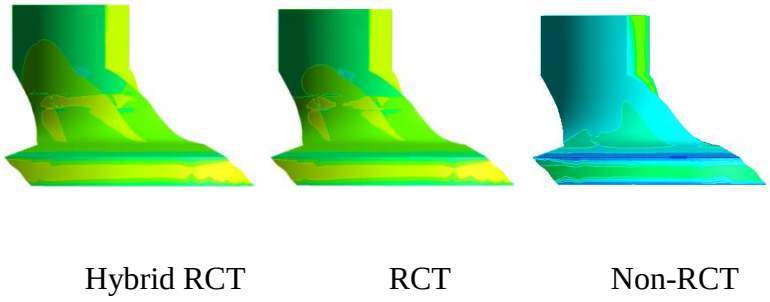

Fig. 101 Impeller Pressure distribution at 140,000rpm and 0.075kg/s

5.2.1.3 Pressure distribution at mass flow rate equal to 0.10kg/s

At the 0.10kg/s mass flow rate condition, three type compressors have the similar pressure distribution at the volute part and impeller part as shown in Figure 102 to Figure 104. The can prove that in this working condition, all type compressors might work very stable.

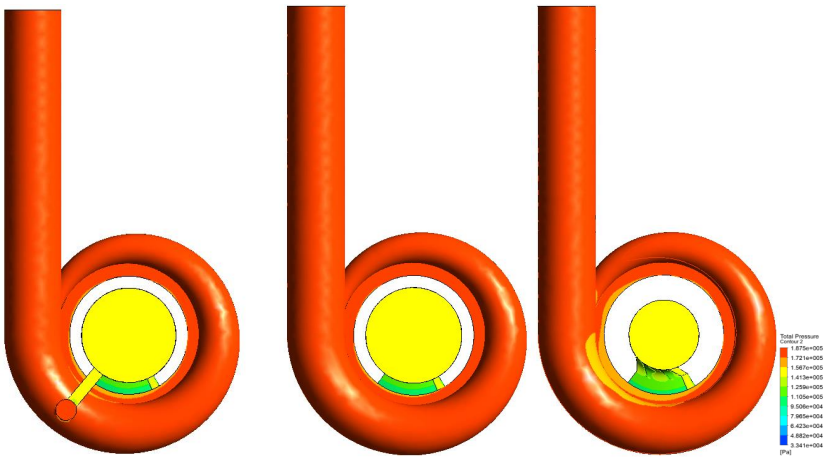

Hybrid RCT RCT Non-RCT

Fig. 102 Compressor Pressure distribution at 140,000rpm and 0.10kg/s

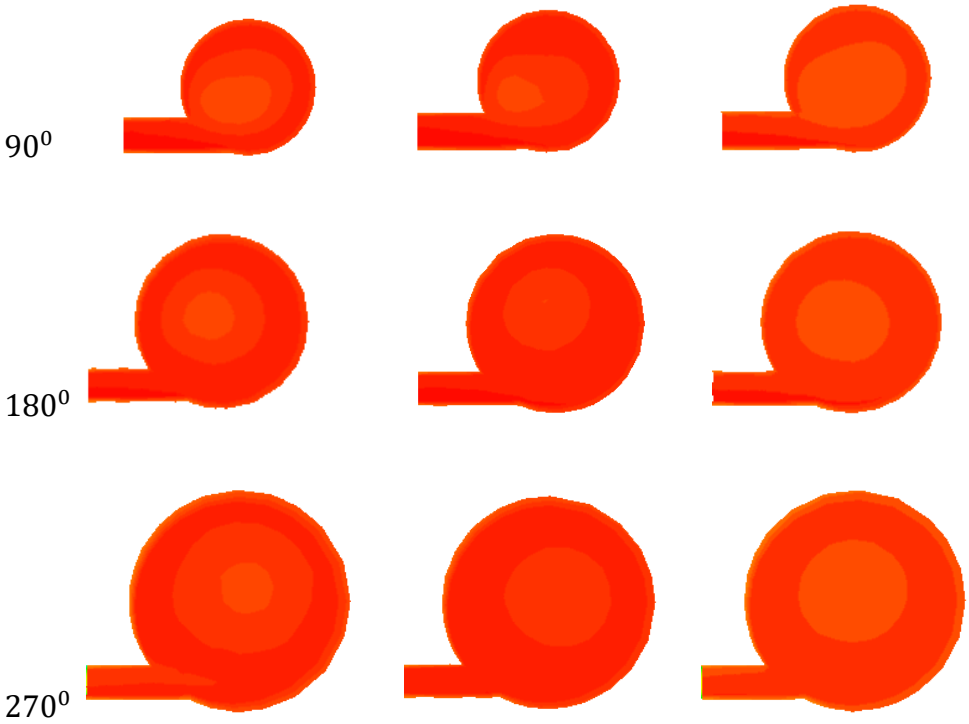

Hybrid RCT RCT Non-RCT

Fig. 103 Compressor Pressure distribution in each cross-section of volute at 140,000rpm and 0.10kg/s

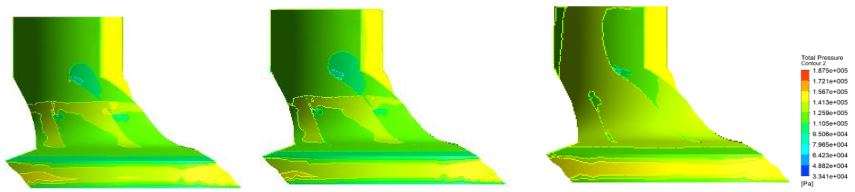

Hybrid RCT RCT Non-RCT

Fig. 104 Impeller Pressure distribution at 140,000rpm and 0.10kg/s

5.2.1.4 Pressure distribution at mass flow rate equal to 0.11kg/s

At the highest efficiency point, the Hybrid RCT compressor has a similar pressure distribution with Non-RCT compressor at the volute part which is shown in Figure 105. In Figure 106 and Figure 107 indicate the Non- RCT has the most uniform pressure distribution inside the volute and impeller among all type compressors.

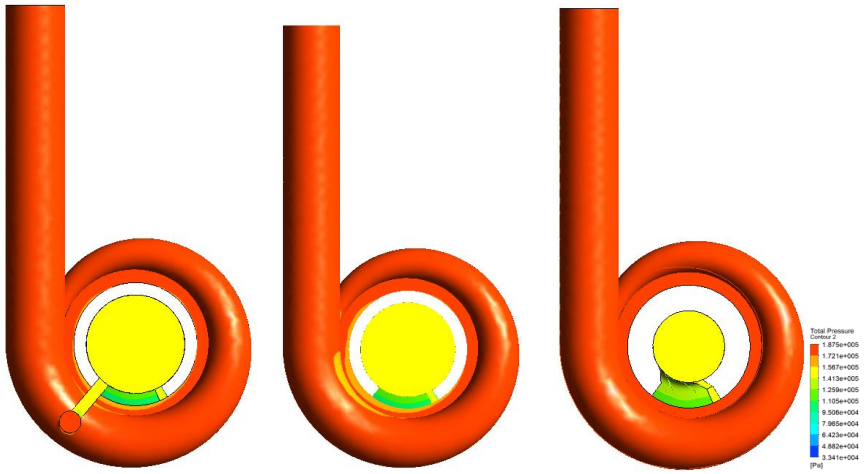

Hybrid RCT RCT Non-RCT

Fig. 105 Compressor Pressure distribution at 140,000rpm and 0.11kg/s

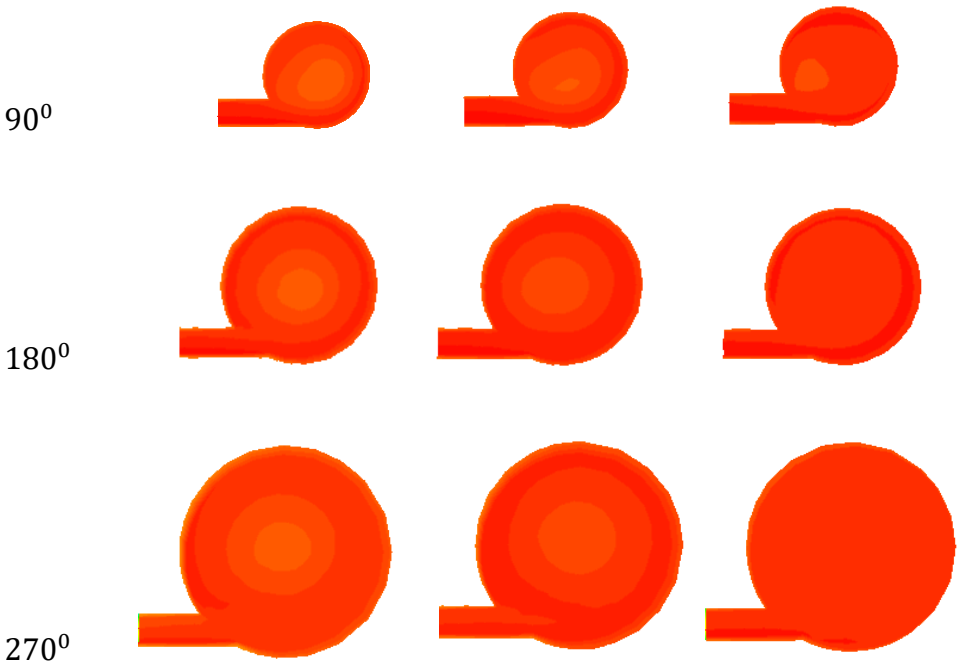

360^0

Hybrid RCT RCT Non-RCT

Fig. 106 Compressor Pressure distribution in each cross section of volute at 140,000rpm and 0.11kg/s

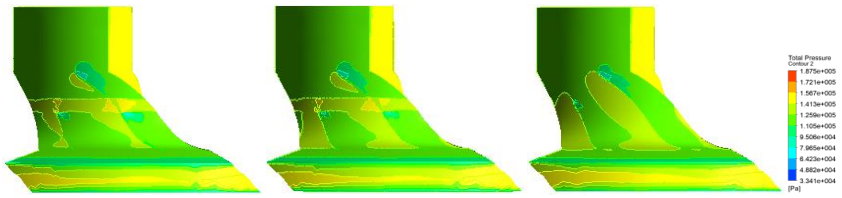

Hybrid RCT RCT Non-RCT

Fig. 107 Impeller Pressure distribution at 140,000rpm and 0.11kg/s

5.2.2 Velocity Vector

5.2.2.1Velocity vector at mass flow rate equal to 0.05kg/s

Figure 108 shows that the Hybrid RCT and RCT compressor can decrease the vortex between impeller blades. When the impeller vortex became smaller, the inlet duct airflow can come into the impeller more straightly. And the Hybrid RCT has the more straightly flow inside the compressor

inlet duct, which is shown in Figure 109 and Figure 110.

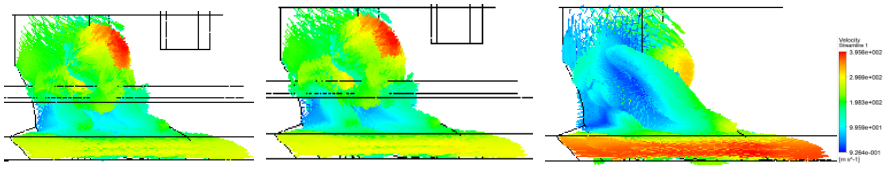

Hybrid RCT RCT Non-RCT

Fig. 108 Impeller velocity vector at 140,000rpm and 0.05kg/s

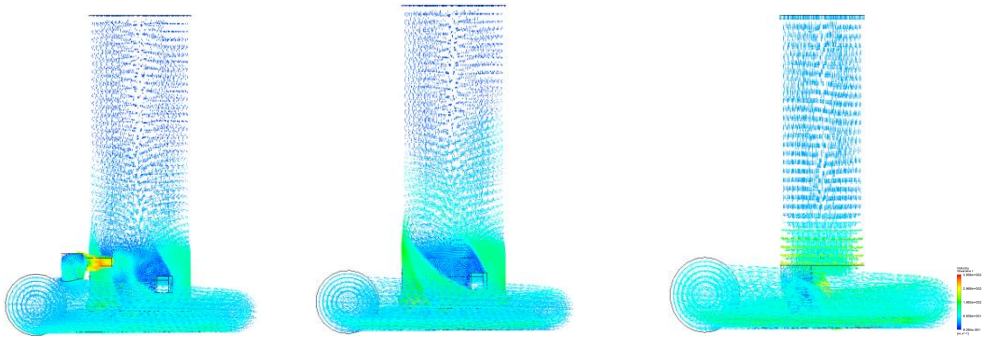

Hybrid RCT RCT Non-RCT

Fig. 109 Inlet duct velocity vector at 140,000rpm and 0.05kg/s

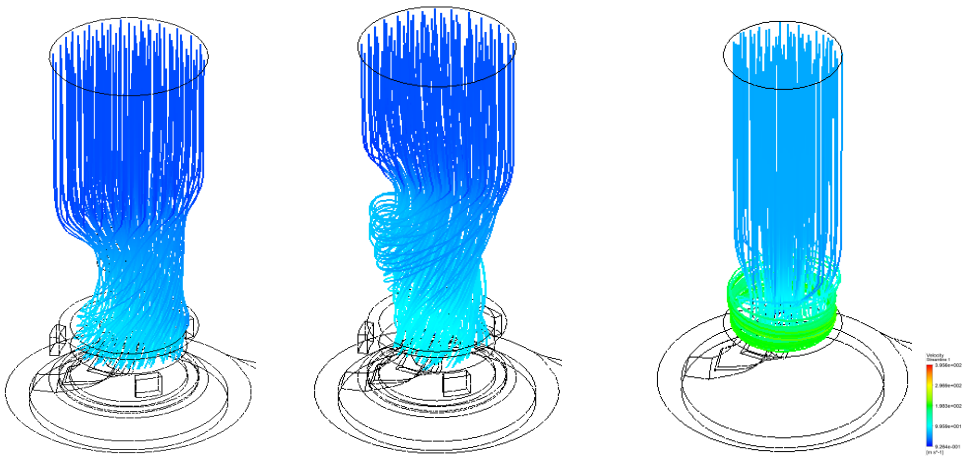

Hybrid RCT RCT Non-RCT

Fig. 110 Inlet duct streamline at 140,000rpm and 0.05kg/s

5.2.2.2 Velocity vector at mass flow rate equal to 0.075kg/s

In Figure 111, the Non-RCT compressor still has the many small vortexes in the impeller area, the Hybrid RCT and RCT compressor also make the small vortexes reduce inside the impeller. And in the inlet duct of the compressor, the Hybrid and Non-RCT compressor inlet flow become straight but the RCT compressor still has some very smaller the swirl flow between the inlet duct and impeller as shown in Figure 112 and Figure 113.

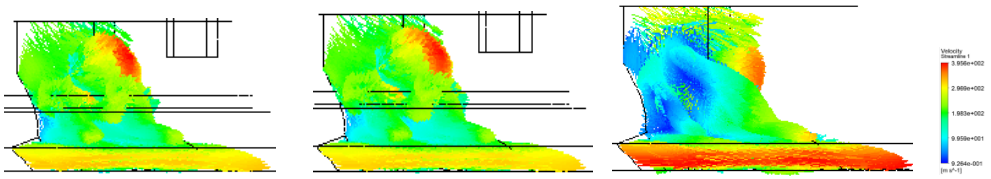

Hybrid RCT RCT Non-RCT

Fig. 111 Impeller velocity vector at 140,000rpm and 0.075kg/s

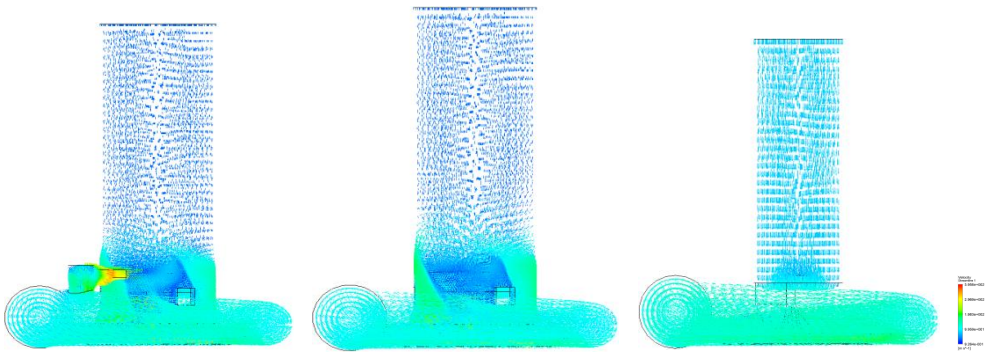

Hybrid RCT RCT Non-RCT

Fig. 112 Inlet duct velocity vector at 140,000rpm and 0.075kg/s

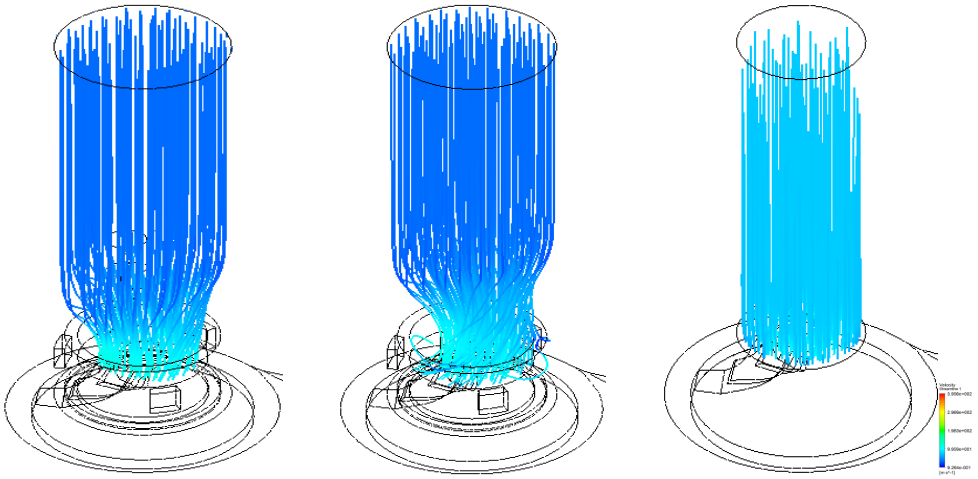

Hybrid RCT RCT Non-RCT

Fig. 113 Inlet duct streamline at 140,000rpm and 0.075kg/s

5.2.2.3 Velocity vector at mass flow rate equal to 0.10kg/s

In this working condition, the Hybrid RCT also can reduce the impeller vortex which is shown in Figure 114. Figure 115 and Figure 116 show that the Hybrid RCT compressor can reduce the influence by the fixed ribs. The flow coming from the volute might mix the swirl flow inside the RCT.

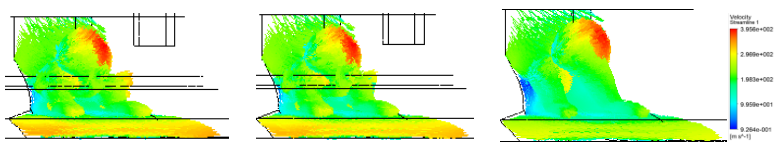

Hybrid RCT RCT Non-RCT

Fig. 114 Impeller velocity vector at 140,000rpm and 0.10kg/s

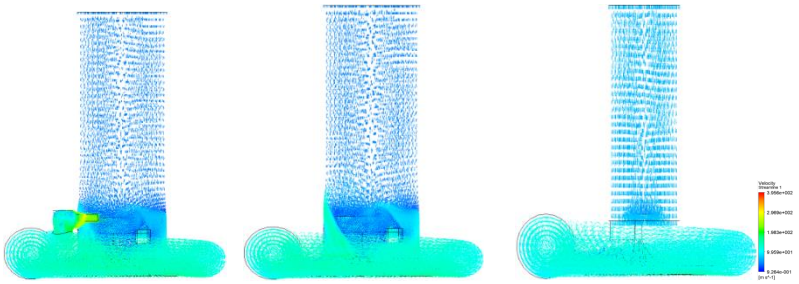

Hybrid RCT RCT Non-RCT

Fig. 115 Inlet duct velocity vector at 140,000rpm and 0.10kg/s

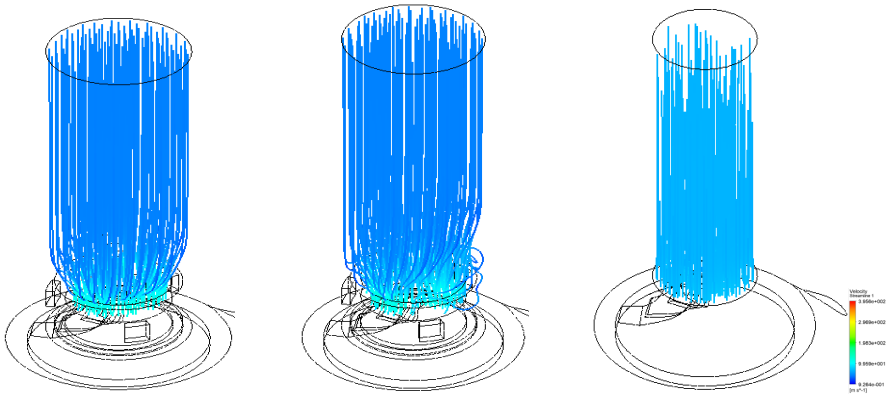

Hybrid RCT RCT Non-RCT

Fig. 116 Inlet duct streamline at 140,000rpm and 0.10kg/s

5.2.2.4Velocity vector at mass flow rate equal to 0.11kg/s

In the highest compressor efficiency point, the Hybrid RCT and RCT compressor no more can avoid the low-velocity area. They have similar impeller velocity vector like the Non-RCT compressor impeller as shown in Figure 117. Figure 118 indicates the RCT compressor has the larger swirl

flow vector inside the RCT part than the Hybrid-RCT compressor. All type compressor inlet duct airflow becomes straightly in this operating condition which is shown in Figure 119.

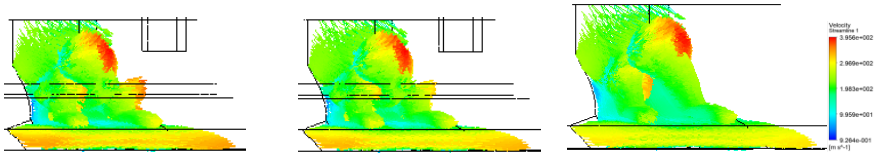

Hybrid RCT RCT Non-RCT

Fig. 117 Impeller velocity vector at 140,000rpm and 0.11kg/s

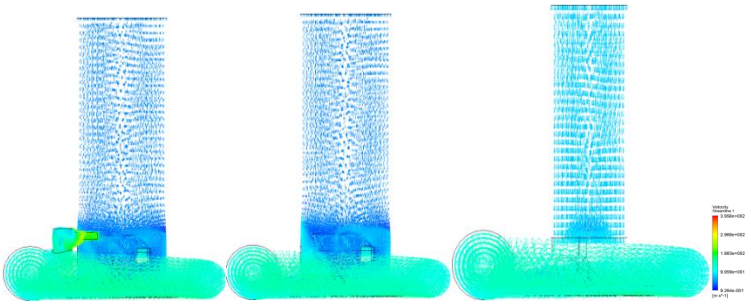

Hybrid RCT RCT Non-RCT

Fig. 118 Inlet duct velocity vector at 140,000rpm and 0.11kg/s

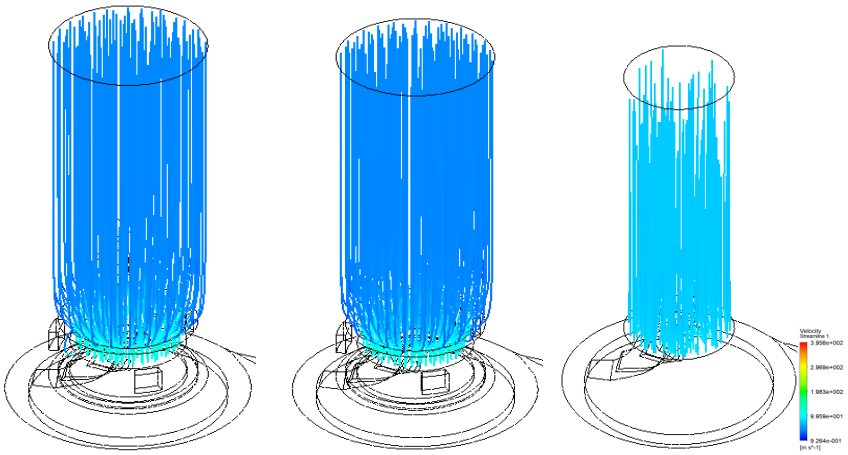

Hybrid RCT RCT Non-RCT

Fig. 119 Inlet duct streamline at 140,000rpm and 0.11kg/s

5.2.3 Compressor map (Pressure Ratio, Efficiency, Surge margin)

The Hybrid RCT compressor surge margin data is 0.83 which is the same with the RCT compressor. But the Hybrid RCT can increase the efficiency at the middle mass flow range which can show in Figure 120 and Figure 121. All Hybrid RCT pressor ratio and efficiency data were shown in Table 12 and Table 13.

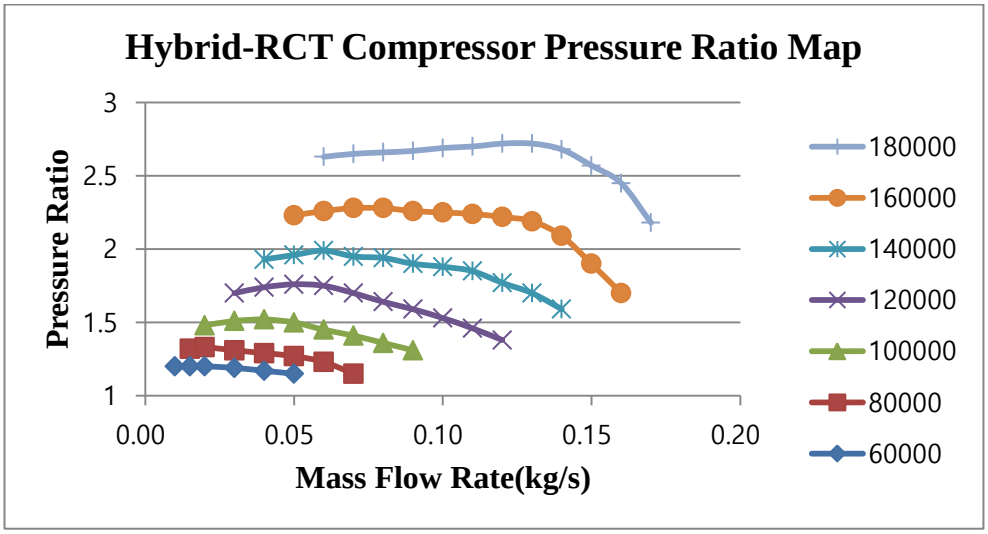

Fig. 120 Hybrid RCT Compressor Pressure Ratio Map

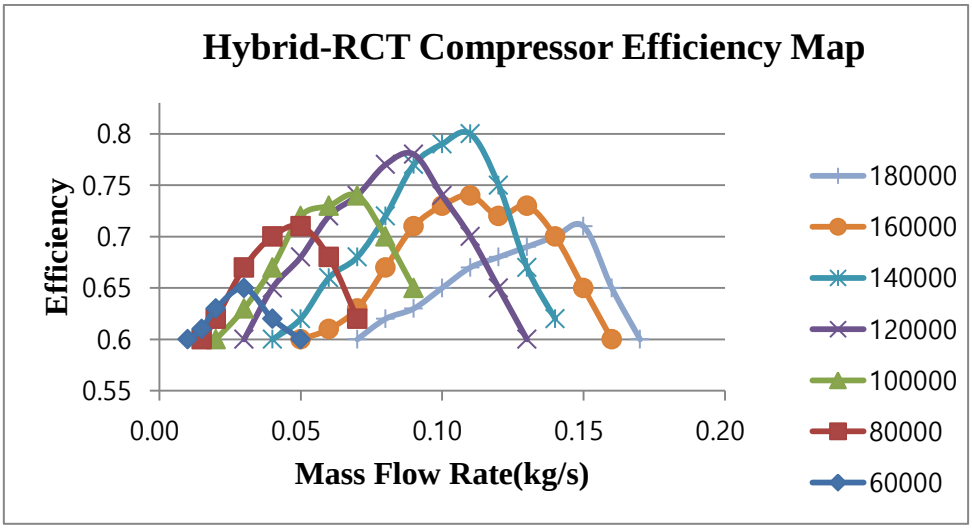

Fig. 121 Hybrid RCT Compressor Efficiency Map

Table. 12 Hybrid RCT Compressor Pressure Ratio data

Mass Flow Rate	60,000	80,000	100,000	120,000	140,000	160,000	180,000
0.01	1.20						
0.015	1.20	1.32					
0.02	1.19	1.32	1.48				
0.03	1.18	1.31	1.51	1.70			
0.04	1.16	1.28	1.53	1.73	1.93		
0.05	1.15	1.27	1.50	1.76	1.98	2.22	
0.06		1.22	1.46	1.76	2.00	2.25	2.63
0.07		1.15	1.40	1.70	1.96	2.28	2.64
0.08			1.36	1.64	1.94	2.27	2.65
0.09			1.30	1.58	1.91	2.27	2.67
0.10				1.52	1.87	2.25	2.68
0.11				1.45	1.85	2.23	2.70

0.12				1.38	1.76	2.22	2.70
0.13					1.70	2.19	2.70
0.14					1.58	2.08	2.67
0.15						1.90	2.56
0.16						1.70	2.45
0.17							2.16

Table. 13 Hybrid RCT Compressor Efficiency data

Mass Flow Rate	60,000	80,000	100,000	120,000	140,000	160,000	180,000
0.01	0.6						
0.02	0.61	0.6					
0.02	0.63	0.62	0.6				
0.03	0.65	0.67	0.63	0.6			
0.04	0.62	0.7	0.67	0.65	0.6		

0.05	0.6	0.71	0.72	0.68	0.62	0.6	
0.06		0.68	0.73	0.72	0.66	0.61	
0.07		0.62	0.74	0.74	0.68	0.63	0.6
0.08			0.7	0.77	0.72	0.67	0.62
0.09			0.65	0.78	0.77	0.71	0.63
0.1				0.74	0.79	0.73	0.65
0.11				0.7	0.8	0.74	0.67
0.12				0.65	0.75	0.72	0.68
0.13				0.6	0.67	0.73	0.69
0.14					0.62	0.7	0.7
0.15						0.65	0.71
0.16						0.6	0.65
0.17							0.6

5.3 Optimization of turbocharger Hybrid compressor

5.3.1 Hybrid RCT connect channel angle

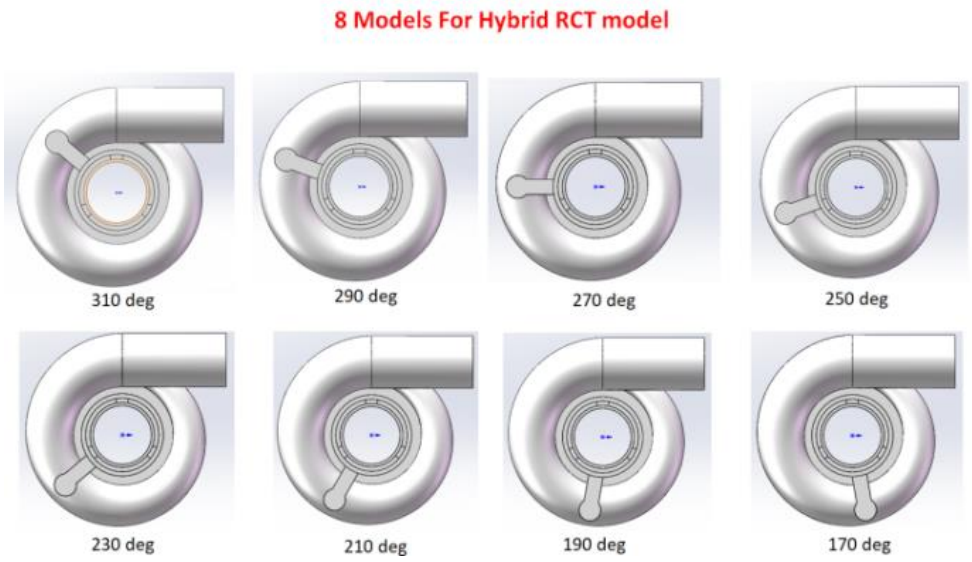

Fig. 122 Hybrid RCT Compressor connecting channel distribution

The Hybrid RCT compressor channel can have a different position at the volute part. In Figure 122 shows 8 positions for Hybrid RCT and then to find which position can get the highest pressure ratio and efficiency at the 140,000rpm and middle range mass flow rate from 0.09kg/s to 0.11kg/. As shown the results from Table 14 to Table 16. The Hyb 270 case (Hybrid RCT connecting channel at the 270-degree position of volute) has the highest data for pressure ratio and efficiency.

Table. 14 Pressure and Efficiency at 140,000rpm and 0.09kg/s for all simulation compressors

m=0.09kg/s	Non-RCT	RCT	Hyb 310	Hyb 290	Hyb 270	Hyb 250	Hyb 230	Hyb 210	Hyb 190	Hyb 170
Pressure Ratio	1.91	1.9	1.91	1.9	1.91	1.9	1.89	1.89	1.9	1.88
Efficiency	0.75	0.71	0.78	0.78	0.79	0.77	0.77	0.78	0.77	0.77

Table. 15 Pressure and Efficiency at 140,000rpm and 0.10kg/s for all simulation compressors

m=0.10kg/s	Non-RCT	RCT	Hyb 310	Hyb 290	Hyb 270	Hyb 250	Hyb 230	Hyb 210	Hyb 190	Hyb 170
Pressure Ratio	1.88	1.88	1.87	1.88	1.88	1.86	1.86	1.85	1.86	1.87
Efficiency	0.78	0.73	0.79	0.79	0.8	0.78	0.78	0.77	0.78	0.78

Table. 16 Pressure and Efficiency at 140,000rpm and 0.11kg/s for all simulation compressors

m=0.11kg/s	Non-RCT	RCT	Hyb 310	Hyb 290	Hyb 270	Hyb 250	Hyb 230	Hyb 210	Hyb 190	Hyb 170
Pressure Ratio	1.85	1.85	1.85	1.85	1.86	1.84	1.85	1.85	1.84	1.85
Efficiency	0.8	0.77	0.8	0.8	0.81	0.79	0.79	0.79	0.78	0.77

5.3.2 Hybrid RCT connect channel size

After choosing the best degree position of Hybrid RCT channel. The channel cutout size should be optimized. The point is the highest efficiency point which the mass flow rate is 0.11kg/s and the RPM is 140,000. The factors are channel cutout height from the diffuser (HH), channel cutout height (Hh) and channel width (Hw). The data is shown in Table 17.

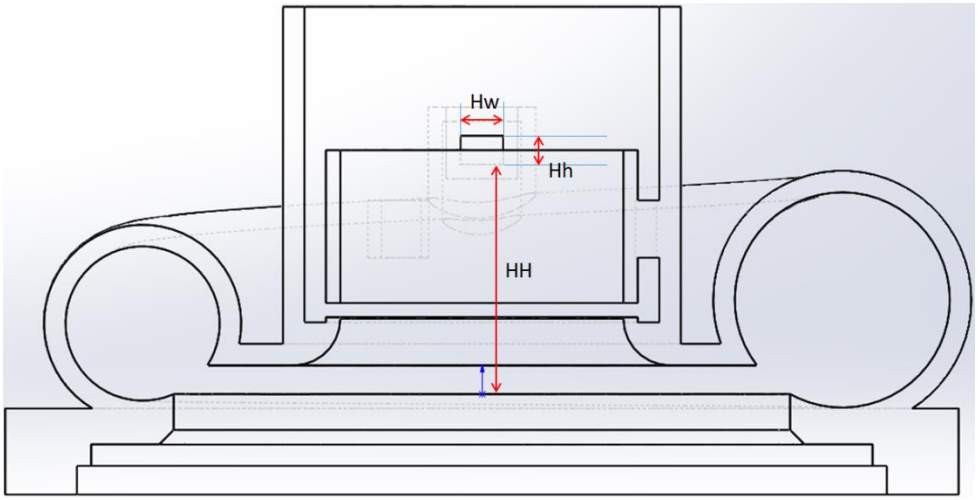

Fig. 123 Hybrid RCT compressor factor for DOE optimization design

Table. 17 Hybrid RCT compressor level data of each factor

Factor	A=HH(mm)	B=Hh(mm)	C=Rw(mm)
Level 1	30	4	4
Level 2	32	6	6
Level 3	34	8	8

After using the Taguchi orthogonal optimum design, the response for pressure ratio results shows in Table 18. The best dimensions for pressure ratio are A1, B3, and C2 which is HH=30mm, Hh=8mm and Rw=6mm. The channel cutout height from the diffuser (HH) is more sensitivity for the compressor pressure ratio which is shown in Figure 124. From Table 19, for the highest efficiency, the best choice for the dimension is A1.5, B1.5, and C3 which means HH=31mm, Hh=5mm and Rw=8mm. And all factors have the sensitivity for the efficiency. In this Hybrid RCT compressor, the efficiency also an important factor. The final optimal is A1.5, B1.5, and C2.5 which the real dimensions are HH=31mm, Hh=5mm and Rw=7mm.

Table. 18 Hybrid RCT Response for Pressure Ratio Means

Level	A	B	C
1	1.860	1.867	1.870
2	1.877	1.870	1.867
3	1.870	1.870	1.870
Delta	0.017	0.003	0.003
Rank	1	3	2

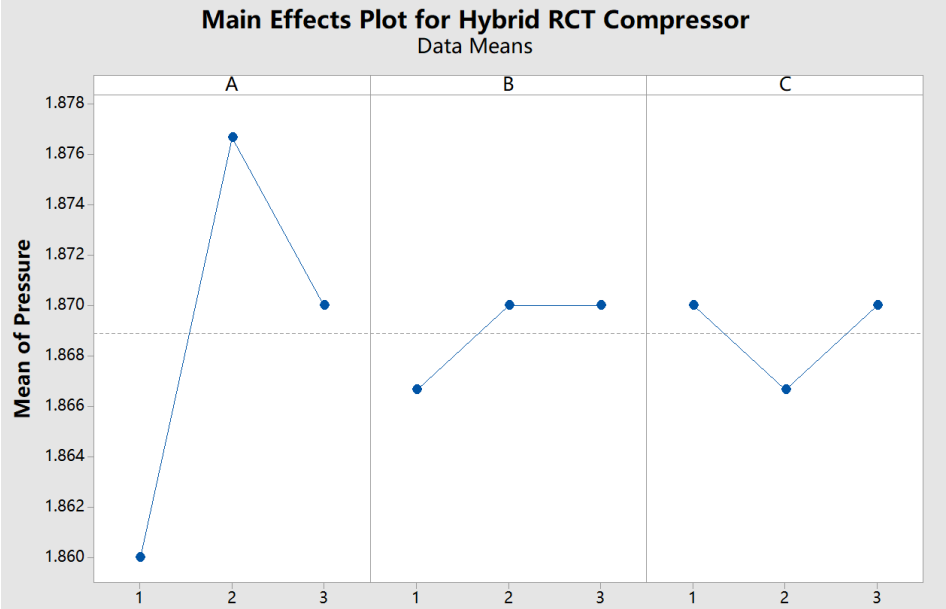

Fig.124 Main mean of pressure ratio effects plot for Hybrid RCT compressor

Table. 19 Hybrid RCT Response for Efficiency Means

Level	A	B	C
1	0.8033	0.8133	0.8000
2	0.8033	0.8033	0.8100
3	0.8133	0.8033	0.8100
Delta	0.0100	0.0100	0.0100
Rank	1.5	1.5	3

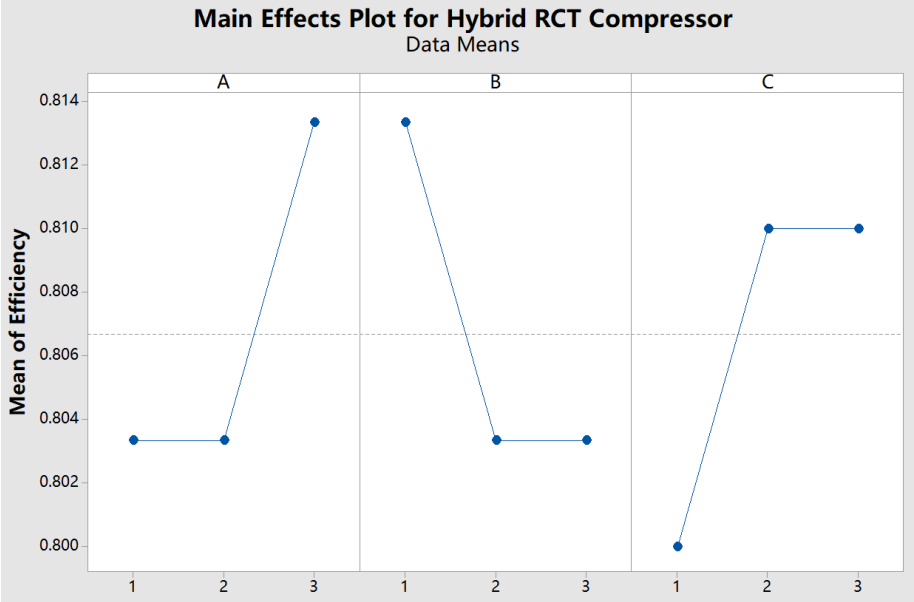

Fig.125 Main mean of efficiency effects plot for Hybrid RCT compressor

5.4 Compressor 3D printer models

For the small size compressor, it is not easy for casting the RCT and Hybrid RCT. The 3D printer is chosen for making the compressor. The materials of a 3D printer are plastic. Figure 126 shows the production process of making the 3D compressor model. And Figure 127 shows the three type 3D printer compressor.

Fig.126 Production process of making the 3D compressor model

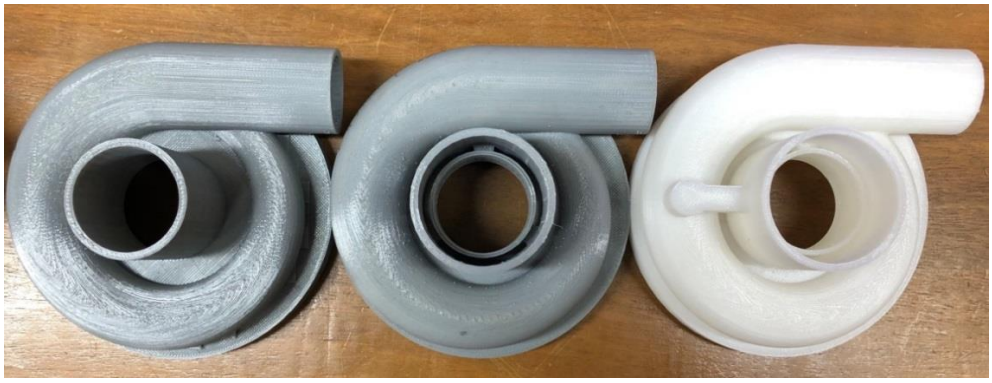

Non-RCT compressor RCT compressor Hybrid RCT compressor

Fig.127 3D printing compressor models

5.5 Summary

A new Hybrid RCT has been designed by the author which has a small channel connecting the compressure volute downstream part and RCT inlet duct to improve the flow movement by overcoming the adverse pressure gradient. The CFD results showed that the Hybrid RCT compressor had a similar performance with the RCT compressor, but it could increase the efficiency than the RCT compressor at the medium mass flow range and showed higher efficiency in a certain region of compressor than the non-RCT compressor.

Chapter 6 Conclusion

In this study, the full range working performance of Non-RCT compressor was obtained by using the CFX simulation software. As analyzing the air flow pressure ratio, velocity vector and streamline inside the compressor with different operating points, the simulation results can show the characteristic of this Non-RCT compressor. The RCT and Hybrid RCT compressor can enhance the compressor operating range. The Non-RCT compressor surge margin data is 0.78, the RCT and Hybrid RCT compressor surge margin data are 0.83. In this Non-RCT compressor, at the low mass flow rate condition, it has the vortex inside the impeller and swirls flow of the downstream of the inlet duct. There are the reasons make the Non-RCT compressor has low efficiency. Comparing the CFD results between the Non-RCT and RCT compressor model, the RCT compressor can increase the efficiency of 3% to 4% at the low mass flow rate, which improves the unstable flow performance. However, at the medium mass flow rate range, especially the mass flow rate of the gasoline engine at the highest power output point, the RCT compressor has the 2% lower efficiency than the non-RCT compressor. A new Hybrid RCT has been designing by the author which has a small channel connecting the compressure volute downstream part and RCT inlet duct to improve the flow movement by overcoming the adverse pressure gradient. The CFD results showed that the Hybrid RCT compressor had a similar performance with the RCT compressor, but it

could increase the efficiency 2% to 3% than the RCT compressor at the medium mass flow range and showed higher efficiency in a certain region of compressor than the non-RCT compressor. The 3D printers were successful to make for three type compressors. In the future, using the metal 3D printing technology, the 3D metal compressor will be made and test in the small displacemnt gasoline engine.

REFERENCES

[1] B. J. Lim and D. H. Rhee, "Research and Development Trends of High Altitude Long Endurance UAV Using Hydrogen Reciprocating Engine," *Current Industrial and Technologic Trends in Aerospace,* 13(1) 179~186, 2015.

[2] Y. S. Kang, B. J. Lim, and J. K. Kim, "Establishment of Multi-stage Turbocharger Layout for HALE UAV Engine and Its Performance Assessment," *The KSFM Journal of Fluid Machinery*, 18(6) 31~36, 2015.

[3] Y. S. Kang, B. J. Lim, and B. J. Cha, "Multi-stage Turbocharger System Analysis Method for High Altitude UAV Engine," *Journal of Mechanical Science and Technology*, 31(6) 2803~2811, 2017.

[4] R. E. Wilkinson, "Design and Development of the Voyager 200/300 Liquid Cooled Aircraft Engine," *General Aviation Aircraft Meeting and Exposition*, Kansas, USA , 1987.

[5] R. E. Wilkinson, R. B. Benway, "Liquid Cooled Turbo-charged Propulsion System for HALE Application," *International Gas Turbine and Aeroengine Congress and Exposition*, ASME 91-GT-399 , 1991.

[6] S. O. Jun, B. J. Lim, and Y. S. Kang, "The Effects of Operating Altitude on the Performance of the Ported Shroud Centrifugal Compressor," *The KSFM Journal of Fluid Machinery*, 20(4) 31~36, 2017.

[7] M. Babák, and Z. Palát, "Design optimization and test of advanced small scale compressor," *European Workshop on New Aero Engine Concepts*, Munich, Germany ,2010.

[8] P. Gao, Y. Zhang, and S. Zhang, "Numerical investigation of the different casing treatment in a centrifugal compressor," *2010 Asia-Pacific Conference on Wearable Computing Systems*, Shenzhen, China , 2010.

[9] H. W. Kim, J. H. Chung, S. H. Ryu, and G. S. Lee, "Numerical and Experimental Study on the Surge Performance Improvement by the Bleed Slot Casing of a Centrifugal Compressor, " *The KSFM Journal of Fluid Machinery*, 18(2) 22~28, 2015.

[10] C. Y. Park, Y. S. Choi, K. Y. Lee, and J. Y. Yoon, "Numerical study on

the range enhancement of a centrifugal compressor with a ring groove system," *Journal of Mechanical Science and Technology*, 26(5) 1371~1378, 2012.

[11] X. Zheng, Y. Zhang, M. Yang, T. Bamba, and H. Tamaki, "Stability Improvement of High-Pressure-Ratio Turbocharger Centrifugal Compressor by Asymmetrical Flow Control—Part II: Nonaxisymmetrical Self-Recirculation Casing Treatment," *Journal of Turbomachinery*, 135 021007-1~8, 2013.

[12] *Turbocharger Guide*, Volume 7, Torrance, CA, Garrett by Honeywell.

[13] X. Huang, H. Chen, and S. Fu, "CFD Investigation on the Circumferential Grooves Casing Treatment of Transonic Compressor," *ASME Turbo Expo*, GT 2008-51107, 2008.

[14] T. Wang, W. Xu, C. Gu, and C. Xiao, "A New Type of Self-adaptive Casing Treatment for a Centrifugal Compressor," *ASME Turbo Expo*, GT 2010-23457, 2010.

[15] W. Knecht, "Diesel engine development in view of reduced emission standards," *Energy*, vol.33, pp. 264-271, 2// 2008.

[16] C. Rodgers, "Centrifugal Compressor Inlet Guide Vanes for Increased Surge Margin," *Journal of Turbomachinery*, vol. 113, p. 696, 1991.

[17] A. Whitfield and A. H. Abdullah, "The performance of a centrifugal compressor with high inlet prewhirl," *Journal of Turbomachinery*, vol. 120, pp. 487-493, 1998.

[18] I. MacDougal and R. L. Elder, "Improvement of operating range in a small, high speed, centrifugal compressor using casing treatments," in *I Mech E Conference Publications (Institution of Mechanical Engineers*), 1982, pp. 19-26.

[19] P. A. Eynon, A. Whitfield, M. R. Firth, A. J. Parkes, and R. Saxton, *A study of the flow characteristics in the inducer bleed slot of a centrifugal compressor.* New York: The American Society of Mechanical Engineers, 1996.

[20] F. B. Fisher, "Application of Map Width Enhancement Devices to Turbocharger Compressor Stages," 1988.

[21] M. Yang, R. Martinez-Botas, Y. Zhang, and X. Zheng, "Effect of Self-Recirculation-Casing Treatment on High Pressure Ratio Centrifugal Compressor," *Journal of Propulsion and Power*, pp. 1-9, 2016.

[22] X. Zheng and C. Lan, "Improvement in the performance of a high-pressure-ratio turbocharger centrifugal compressor by blade bowing and self-recirculation casing treatment," *Proceedings of the Institution of Mechanical Engineers, Part D: Journal of Automobile Engineering*, vol. 228, pp. 73-84, 2014.

[23] W. Jansen, A. Carter, and M. Swarden, "Improvements in surge margin for centrifugal compressors," *AGARD Centrifugal Compressors, Flow Phenomena and Performance* 17 p(SEE N 81-17447 08-37), 1980.

[24] S. Sivagnanasundaram, S. Spence, J. Early, and B. Nikpour, "Experimental and numerical analysis of a classical bleed slot system for a turbocharger compressor," *Proceedings of IMechE 10th International Conference on Turbochargers and Turbocharging*, ed, 2012, pp. 325-341.

[25] S. Sivagnanasundaram, S. Spence, and J. Early, "Map Width Enhancement Technique for a Turbocharger Compressor," *Journal of Turbomachinery*, vol. 136, pp. 061002-061002, 2013.

[26] H. Tamaki, "Effect of Recirculation Device With Counter Swirl Vane on Performance of High Pressure Ratio Centrifugal Compressor," *Journal of Turbomachinery*, vol. 134, pp. 051036-051036, 2012.

[27] G. A. Christou, "Fluid mechanics of ported shroud centrifugal compressor for vehicular turbocharger applications," Ph. D., Massachusetts Institute of Technology. Department of Aeronautics and Astronautics., Massachusetts Institute of Technology, Massachusetts, 2015.

[28] B. Semlitsch, V. Jyothishkumar, M. Mihaescu, L. Fuchs, E. Gutmark, and M. Gancedo, "Numerical flow analysis of a centrifugal compressor with ported and without ported shroud," *SAE Technical Papers*, vol. 1, 2014.

[29] H. Chen and V.-M. Lei, "Casing Treatment and Inlet Swirl of Centrifugal Compressors," *Journal of Turbomachinery*, vol. 135, p. 041010, 2013.

[30] A. C. A. Research, ANSYS CFX-Solver Theory Guide. USA: ANSYS, Inc., 2017.

[31] H. Chen, S. Guo, X. C. Zhu, Z. H. Du, and S. Zhao, "Numerical simulations of onset of volute stall inside a centrifugal compressor," *Proceedings of the ASME Turbo Expo*, 2008.

[32] F. R. Menter, "Two-equation eddy-viscosity turbulence models for engineering applications," *AIAA Journal*, vol. 32, pp. 1598-1605, 1994.

[33] X. Q. Zheng, J. Huenteler, M. Y. Yang, Y. J. Zhang, and T. Bamba, "Influence of the volute on the flow in a centrifugal compressor of a high-pressure ratio turbocharger," *Proceedings of the Institution of Mechanical Engineers, Part A: Journal of Power and Energy*, vol. 224, pp. 1157-1169, 2010.

[34] D. C. Wilcox, *Turbulence modeling for CFD vol. 2*: DCW industries La Canada, CA, 1998.

[35] P. Chow, M. Cross, and K. Pericleous, "A natural extension of the conventional finite volume method into polygonal unstructured meshes for CFD application," *Applied Mathematical Modelling*, vol. 20, pp. 170-183, 1996.

[36] G. Després, G. N. Boum, F. Leboeuf, D. Chalet, P. Chesse, and A. Lefebvre, "Simulation of near surge instabilities onset in a turbocharger compressor," *Proceedings of the Institution of Mechanical Engineers, Part A: Journal of Power and Energy*, vol. 227, pp. 665-673, September 1, 2013.